AN ABSTRACT OF THE THESIS OF

Michael Wai-Hung Chan (Name) for the degree Master of Science (Degree)

in Atmospheric Sciences (Major Department) presented on October 28, 1974 (Date)

Title: DIURNAL FLUCTUATION OF METEOROLOGICAL VARIABLES ABOVE SLOPING TERRAIN

Redacted for privacy

Abstract approved: Larry J. Mahrt

Surface meteorological data collected at a mesonetwork in Colorado during the 1973 National Hail Research Experiment were analyzed to see if a diurnal oscillation of boundary layer wind exists and also to determine the mechanism that drives the wind system. The average temperature, pressure, and wind velocity for a month's time were computed in order to filter out synoptic disturbances.

The analysis of averaged daily potential temperature distribution shows that, during the study period, air is always stable along the slope at night and is stable over 75% of the time during the daylight hours. This implies that nighttime downslope flow is driven by baroclinity and strongly influenced by frictional effects. This analysis also shows that differences in horizontal potential temperature are minimal at the time of day when hail activity is statistically a maximum.

Hodographs obtained from averaging wind velocities show that the air flow is upslope during the afternoon and downslope at night. This type of air movement is attributed to baroclinicity caused by diurnal heating along a slope.

Spectral analysis of wind speeds at two stations shows numerous peaks and valleys in various spectra. Several of these peaks are attributed to diurnal and inertial oscillations.

Diurnal Fluctuation of Meteorological Variables Above Sloping Terrain

by

Michael Wai-Hung Chan

A THESIS

submitted to

Oregon State University

in partial fulfillment of
the requirements for the
degree of

Master of Science

Completed October 28, 1974

Commencement June 1975

APPROVED:

Redacted for privacy

Professor of Atmospheric Sciences

in charge of major

Redacted for privacy

Chairman of Department of Atmospheric Sciences

Redacted for privacy

Dean of Graduate School

Date thesis is presented October 28, 1974

Typed by Clover Redfern for Michael Wai-Hung Chan

ACKNOWLEDGMENTS

I would like to thank my major professor, Dr. Larry J. Mahrt for his many helpful suggestions, his professional guidance and his encouragement throughout this study.

I also wish to thank Dr. Ernest Peterson and Dr. Clayton Paulson for their advice and for reviewing the manuscript.

This research has been supported by the National Hail Research Experiment under Subcontract No. NCAR 27-73. Data for this study was also provided by the NHRE group at National Center for Atmospheric Research, Boulder, Colorado.

TABLE OF CONTENTS

LIST OF FIGURES

LIST OF TABLES

DIURNAL FLUCTUATION OF METEOROLOGICAL VARIABLES ABOVE SLOPING TERRAIN

I. INTRODUCTION

The objectives of the National Hail Research Experiment (NHRE) are:

1) To gain an increased understanding, by observation and analysis of surface and upper-air meteorological data, of the physics governing the generation of convective storms that product hailfall at the ground, and
2) Equipped with this increased knowledge, to develop, if possible, a practicable method for suppressing the occurrence of damaging hail.

Although generation of convective systems associated with hailstorms are usually a direct result of synoptic disturbances, local terrain and boundary layer effects may be important in determining the particular location and intensity of the convective activity. The following are some of these effects:

1) Direct uplifting by sloped terrain.
2) Baroclinic circulations associated with heating over sloped terrain and local modification of thermodynamic stability.
3) Frictionally induced low level convergence (divergence).

The goal of this thesis is to assess the importance of the first and second effects by analyzing data collected in July during the 1973 National Hail Research Experiment.

Temperature and pressure readings were extracted from stripcharts while wind direction and speed readings were taken from microfilm stripcharts. Unfortunately, there is no vertical resolution in temperature and wind direction and speed because the stations measure only surface meteorological variables.

The National Hail Research Experiment has a mesonetwork consisting of 33 stations located in northeastern Colorado and southwestern Nebraska. Data from six of these stations situated along a gentle slope in a north-south direction are used in this study. Ground cover is homogeneous for five of the stations. They lie in regions of sparse open range type vegetation. The sixth station is located adjacent to an asphalt airstrip in Kimball. The Rocky Mountains are to the west of this mesonetwork and to the east lie the Great Plains. Such topography will have a significant influence on the wind flow pattern as is discussed later in this thesis.

The first section of this thesis consists of a review of findings by various researchers that have a bearing on this study. Then a small section gives a general picture of the observational field program. This is followed by a stability analysis, a wind analysis, a thermal wind calculation using an order of magnitude argument, and

finally, a harmonic and a spectral analysis of the wind field. A summary of the results of this data analysis is presented in the section Summary and Conclusions.

II. LITERATURE REVIEW

Many theoretical studies on diurnal wind oscillations in the boundary layer have been made. Estoque (1963) investigated the response of wind and temperature fields to a temperature wave imposed at the ground, assuming that horizontal advection is negligible. His model consists of a surface layer, above a flat terrain, in which the vertical fluxes of heat, momentum and moisture are constant with height and an upper layer where the influence of turbulent transfer processes gradually decrease with height. The driving force in the model is radiation--both short and long wave. The general features of the temperature variations observed by Estoque appear to be predicted satisfactorily by the model. Some discrepancy between the prediction and observations exists in the temperature distribution at dawn for which the prediction shows a stronger inversion than the observations in the layer between the surface and the 400 m level. This could possibly result from the omission of horizontal advection. The predicted wind field shows the characteristic diurnal variation of the speed at different levels. Near the 600 m level, the maximum wind (so called low level jet) occurs at night and the minimum occurs shortly before noon. At 10 m above the ground, the maximum is predicted to occur at 1300 local time and lighter winds occur at night.

Krishna (1968) modified Estoque's model by introducing similarity theories, expressing the nondimensional wind shear and lapse rate as functions of the nondimensional height z/L, where L is the Monin-Obukhov length, and formulating K, the eddy viscosity, as a function of u_* and z/L. He concluded that the phase angle of the diurnally varying wind speed wave shifts with height, the rate of shift varying with latitude--negative at latitudes north of 30°N, zero at about 30°N and positive south of 30°N. The low level wind maximum occurs before midnight in midlatitudes, slightly after midnight at 30°N, at sunrise at 17.5°N and later further south. The amplitude of the diurnal wind speed wave increases from north to south, reaches a maximum a little below 30°N, and then decreases rapidly. Winds attain an absolute minimum value by sunrise north of 30°N, and only a relative minimum by about sunset south of 30°N. A semi-diurnal oscillation of wind speed occurs in the layers below 400 m north of 30°N, but is not noticed at latitudes of 30°N.

Following theoretical works of Estoque and Krishna, Paegle (1970) obtained a diurnal speed oscillation of the boundary layer winds using a model with diurnally periodic eddy viscosity. The observed flow is reproduced in a simple, one dimensional inhomogeneous, boundary layer model employing gradient diffusion.

$$\frac{\partial W}{\partial t} - \frac{\partial^2 W}{\partial \zeta^2} = G(\zeta, t) \qquad \text{where} \quad W = u + iv$$

ζ and t are nondimensional variables

$$\zeta = \left(\frac{f}{k}\right)^{1/2} z$$

$$t = ft'$$

and

$$k = A(1 - \nu \cos(\omega t')),$$

ω = diurnal frequency, $\nu \leq 1$

The geostrophic wind at 2000 m is imposed as the upper boundary condition. It appears that the linearized model with variable viscosity and variable geostrophic wind describes quite closely the mean oscillation over the Great Plains, predicting a night-time, pre-dawn occurrence of speed maxima. One drawback of the model is that it fails to account for the very large supergeostrophic speeds occasionally observed. At any rate, Peagle's model probably explains the secondary wind maximum evident in the NHRE data, to be presented in subsequent section.

Holton (1967) made a detailed theoretical study of the diurnal oscillation of boundary layer wind above sloping terrain. His model uses a coordinate system (χ, y, ζ) in which χ is tangent to the ground in the x-z cartesian plane and ζ is normal to the ground. His equations consist of the full equations of motion, the continuity

equation and the thermodynamic energy equation. He noted that because the gravitational force vector has a component parallel to a sloping boundary, the diurnal oscillation of temperature in the boundary layer provides a source of potential energy which drives a diurnal oscillation in the boundary layer wind. Thus, the Ekman boundary layer and the thermal boundary are coupled. His model found that the thermal forcing mechanism can account for the amplitude of the nocturnal low-level jet observed over the sloping Great Plains region of the United States. Discrepancies with the actual observations are attributed by Holton to the use of a constant eddy viscosity.

Apart from theoretical studies, data analysis of diurnal wind oscillations have also been made by several investigators. Surface wind observations were made in the Kananaskis valley of southwestern Alberta in 1960 (MacHattie, 1967). Hourly values of average speed and direction were resolved into components along and across the valley direction. MacHattie found that surface wind components across the valley have a more pronounced diurnal cycle than components along the valley both for clear days and on monthly averages. It appears that cross valley winds are less susceptible to overriding by synoptic-scale influences than up-and-down valley winds. Although mountain and valley winds arise from radiational influences on mountain slopes, it is possible for these local wind patterns to be less apparent on clear days in summer than days when incoming radiation is less intense.

This is because convective activity and, hence, the coupling of surface wind with the synoptic gradient wind at higher levels tend to be stronger on days of more intense radiation.

Frenzel (1962) examined data collected by 12 observing stations taking hourly observations located along a line oriented approximately northwest-southeast along the San Joaquin Valley for a distance of about 450 miles. He also analyzed data collected at nine other stations located in or near the San Francisco Bay area in California. Data was analyzed for the month of July 1958. In this study, he shows that the low-level diurnal circulation results primarily from the differential heating between land and water, the diabatic heating of sloping terrain and the constraining influence of the topography. Wind coming from the coast enters the valley and is diverted both northward and southward. Pressure differences indicate that air in the valley oscillates in phase with that near the coast. Thus differential heating between land and water and diabatic heating along sloping terrain combine to produce a tertiary circulation which is well developed in depth and areal extent.

III. OBSERVATIONAL PROGRAM

In May 1965, the Interdepartmental Committee for Atmospheric Science recommended to the Federal Council for Science and Technology that hail suppression research be carried out. In December 1968, a proposal for the research prepared by the National Science Foundation was approved by the Interdepartmental Committee for Atmospheric Science. Between 1968 to 1970, hailstorms in northeast Colorado were studied under the sponsorship of the National Science Foundation, by the Joint Hail Research Project, later known as the National Hail Research Experiment.

The first full-scale operation was carried out in the summer of 1972 (Figure 1). In 1973, the surface mesonetwork, where data for this research was collected, was expanded and consisted of 33 stations located in northeastern Colorado and southwestern Nebraska (Figure 2).

Each station in the mesonetwork has a modified African thermal shelter which houses the recording instruments. Wind speed and direction at 10 m above the ground are recorded by a research grade instrument on an analog strip chart. The wind speed transmitter has as accuracy to within one percent of the actual wind speed, and both the speed and direction transmitter have an operating temperature range of -48°C to 67°C.

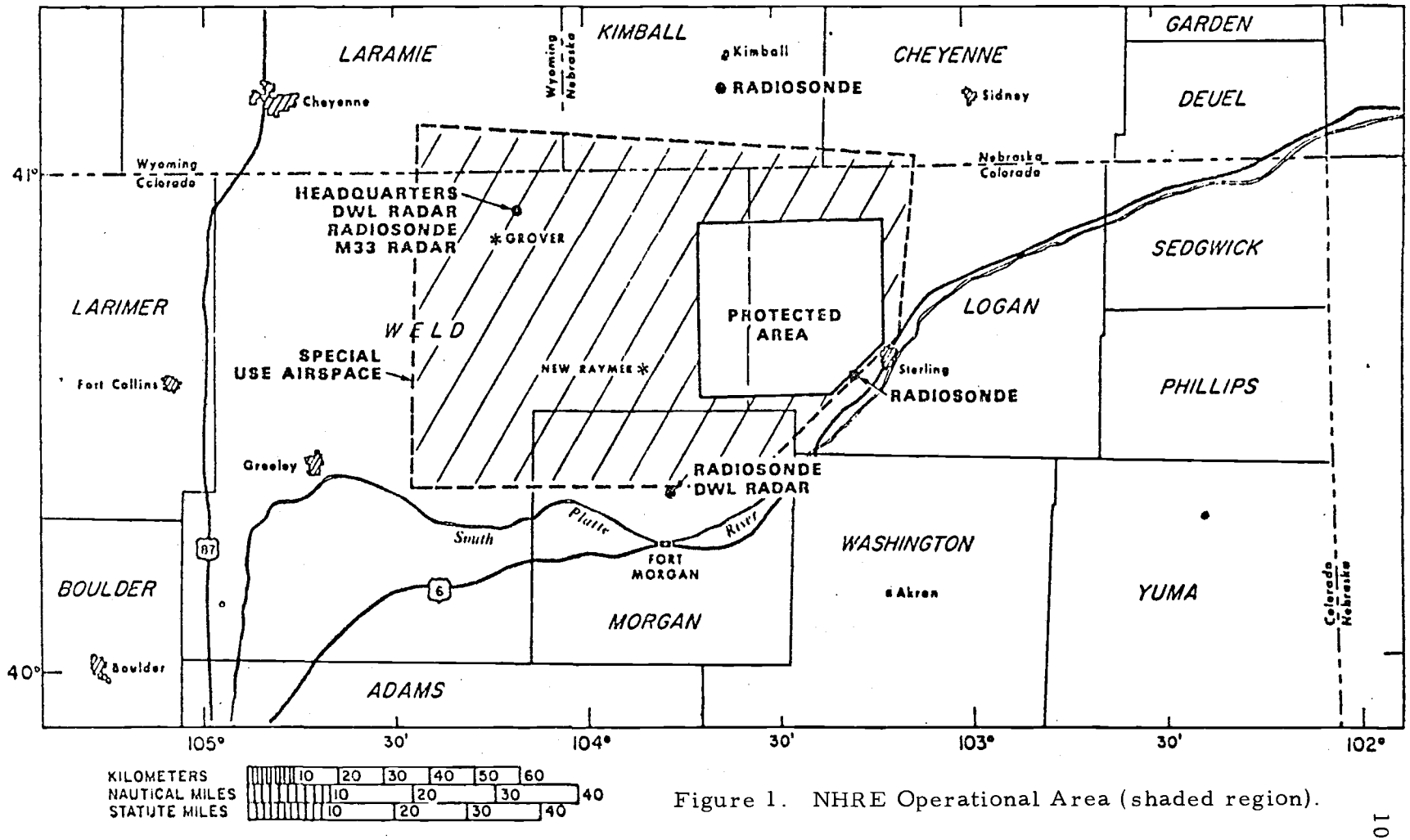

Figure 1. NHRE Operational Area (shaded region).

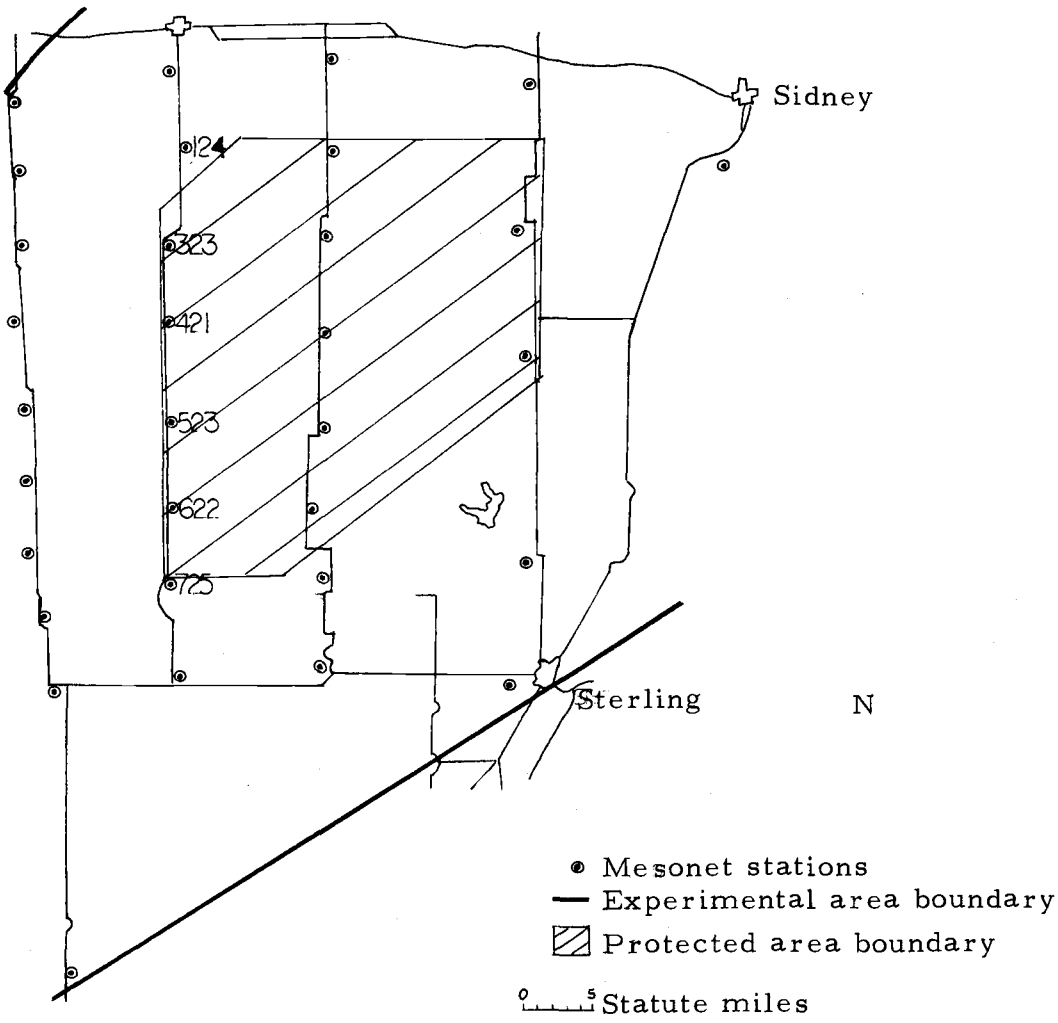

Figure 2. NHRE 1973 Mesonetwork

Temperature at 1.5 m above the ground is recorded by an Epic thermograph having a temperature range of 0°C to 40°C and an accuracy within 0.1°C. A standard Weather Bureau Belfort microbarograph with an accuracy of within 0.1 mb is used to record pressure changes at 1.5 m above the ground. In addition, there is a digital aneroid barometer for correcting the barograph, an Assman aspirator for correcting the thermograph, and a set of maximum and minimum thermometers.

IV. ANALYSIS AND DISCUSSION

A. Stability Analysis

A preliminary five-day (May 26, June 21, July 22, 25, 1972 and July 9, 1971) study of wind, temperature and pressure data from all mesonet stations showed a diurnal oscillation of wind and temperature along a line of stations. These stations (Table 1) were selected for further investigation. They all lie along route 71, which slopes gently upwards from south to north. Station 725 is the southernmost station and 124 is northernmost station. Their aspect is southeast.

Table 1. Mesonet stations.

Station No.	Elevation (m)	Distance Apart (km)	Slope (%)
124	1490		
		10.85	-0.37
323	1530		
		8.35	0.01
421	1523		
		10.45	1.03
523	1415		
		8.04	0.19
622	1400		
		9.15	0.33
725	1370		

Available surface data exist for these stations for the period June 1, 1973 to July 31, 1973. However, out of these 61 days, 38 days of data had to be discarded due to either a lack of a correction factor or indiscernibility of the trace on the chart. In order to be consistent, a day's data was analyzed only when reliable data were

collected at all stations on that day. Consequently, only 23 days of data were classified as reliable.

Table 2. Days of reliable data.

	S	M	T	W	T	F	S
July	1	2	3	4		6	7
	8		10	11	12	13	14
	15		17	18			
		23	24	25	26	27	28
	29	30					

Mean hourly measurements of temperature and pressure, defined as the mean ordinate of a continuous trace (such as appears on a barograph or thermograph) over a period of one hour, were taken from strip charts. From a given temperature and pressure, the potential temperature is computed using Poisson's equation.

The hourly arithmetic mean temperature, pressure and potential temperature for each of the six stations were also calculated (Tables 3, 4, and 5). By averaging over 23 days, synoptic disturbances are eliminated.

To get a better conceptual idea of the daily distribution of meteorological variables, the averaged temperature, pressure and potential temperature at each station are plotted over a 24 hour period. Figure 3 is a plot of the daily temperature distribution for all stations. Figure 4 is a plot of pressure distribution and Figure 5, a plot of potential temperature.

Table 3. Mean temperature (°C) at various mesonet stations.

Time (hr)	Station					
	124	323	421	523	622	725
0	17.1	17.3	18.0	17.8	17.6	18.1
1	16.4	16.5	17.2	17.0	16.9	17.1
2	15.8	15.8	16.3	16.3	16.3	16.3
3	15.1	15.1	15.7	15.8	15.8	15.6
4	14.5	14.6	15.4	15.3	15.2	15.0
5	14.1	14.3	15.3	15.0	14.7	14.6
6	14.9	15.1	15.9	15.5	15.5	14.9
7	17.1	17.3	17.8	17.9	17.8	17.0
8	19.8	19.5	19.5	19.9	19.8	19.6
9	22.5	22.5	21.3	21.7	21.9	21.5
10	24.5	23.8	23.6	24.4	23.5	23.6
11	25.9	25.2	24.8	25.5	25.6	25.7
12	26.9	26.2	25.7	26.7	26.7	26.8
13	27.9	27.0	26.6	27.6	27.5	27.7
14	28.0	27.2	26.8	28.0	28.0	28.3
15	28.3	27.6	27.1	28.2	28.1	28.4
16	28.1	27.5	27.1	28.0	28.0	28.3
17	27.6	27.0	26.6	27.7	27.6	28.1
18	26.4	25.9	25.5	26.7	26.7	27.4
19	24.5	24.1	23.6	24.6	24.7	25.5
20	22.4	21.9	21.8	22.3	22.5	23.0
21	20.4	20.1	20.5	20.5	20.6	21.3
22	19.0	18.9	19.4	19.2	19.4	20.0
23	17.9	18.0	18.7	18.4	18.5	18.9

Table 4. Mean pressure (mb) at various mesonet stations.

Time (hr)	Station					
	124	323	421	523	622	725
0	852.5	849.5	847.4	859.7	861.7	865.0
1	852.5	849.4	847.3	859.7	861.7	865.0
2	852.4	849.3	847.2	859.6	861.5	864.8
3	852.3	849.2	847.1	859.5	861.4	864.8
4	852.4	849.2	847.2	859.5	861.5	864.8
5	852.5	849.3	847.3	859.6	861.6	864.9
6	852.7	849.4	847.5	859.8	861.8	865.2
7	853.0	849.8	847.8	860.2	862.1	865.4
8	853.3	850.1	848.1	860.4	862.3	865.7
9	852.7	849.7	848,1	860.6	862.5	865.9
10	852.6	849.7	847.6	860.0	862.6	866.0
11	852.6	849.8	847.6	860.0	861.9	865.2
12	852.4	849.6	847.4	859.8	861.7	865.0
13	852.0	849.2	847.1	859.4	861.3	864.4
14	851.7	849.0	846.8	859.1	861.0	864.3
15	851.3	848.6	846.5	858.7	860.6	863.9
16	851.1	848.3	846.2	858.4	860.4	863.7
17	851.0	848.2	846.0	858.3	860.2	863.6
18	851.1	848.2	846.1	858.2	860.1	863.5
19	851.3	848.3	846.2	858.4	860.3	863.6
20	851.4	848.5	846.4	848.6	860.5	863.9
21	851.9	848.9	846.8	859.0	860.9	864.3
22	852.2	849.3	847.2	859.5	861.4	864.7
23	852.4	849.3	847.4	859.6	861.5	864.8

Table 5. Mean potential temperature (°K) at various mesonet stations.

Time (hr)	Station					
	124	323	421	523	622	725
0	303.6	304.2	305.1	303.6	303.2	303.4
1	302.9	303.3	304.3	302.8	302.5	302.4
2	302.3	302.6	303.4	302.1	301.9	301.6
3	301.6	301.9	302.7	301.6	301.4	300.8
4	300.9	301.4	302.4	301.1	300.8	300.2
5	300.5	301.0	302.3	300.7	300.2	299.8
6	301.3	301.9	302.9	301.2	301.0	300.1
7	303.6	304.1	304.9	303.7	303.4	302.2
8	306.4	306.4	306.6	305.8	305.5	304.9
9	309.3	309.6	308.5	307.6	307.6	306.9
10	311.4	311.0	311.0	310.5	309.3	309.1
11	312.8	312.4	312.2	311.7	311.6	311.3
12	313.9	313.5	313.2	312.9	312.7	312.5
13	315.0	314.4	314.2	313.9	313.6	313.5
14	315.1	314.6	314.4	314.4	314.2	314.1
15	315.5	315.1	314.7	314.6	314.3	314.3
16	315.3	315.0	314.8	314.4	314.2	314.2
17	314.8	314.5	314.3	314.1	313.8	314.0
18	313.5	313.3	313.1	313.1	312.9	313.3
19	311.5	311.4	311.1	310.9	310.8	311.3
20	309.3	309.1	309.2	308.5	308.5	308.6
21	307.2	307.2	307.8	306.5	306.4	306.8
22	305.7	305.9	306.6	305.1	305.1	305.4
23	304.5	304.9	305.8	304.3	304.2	304.3

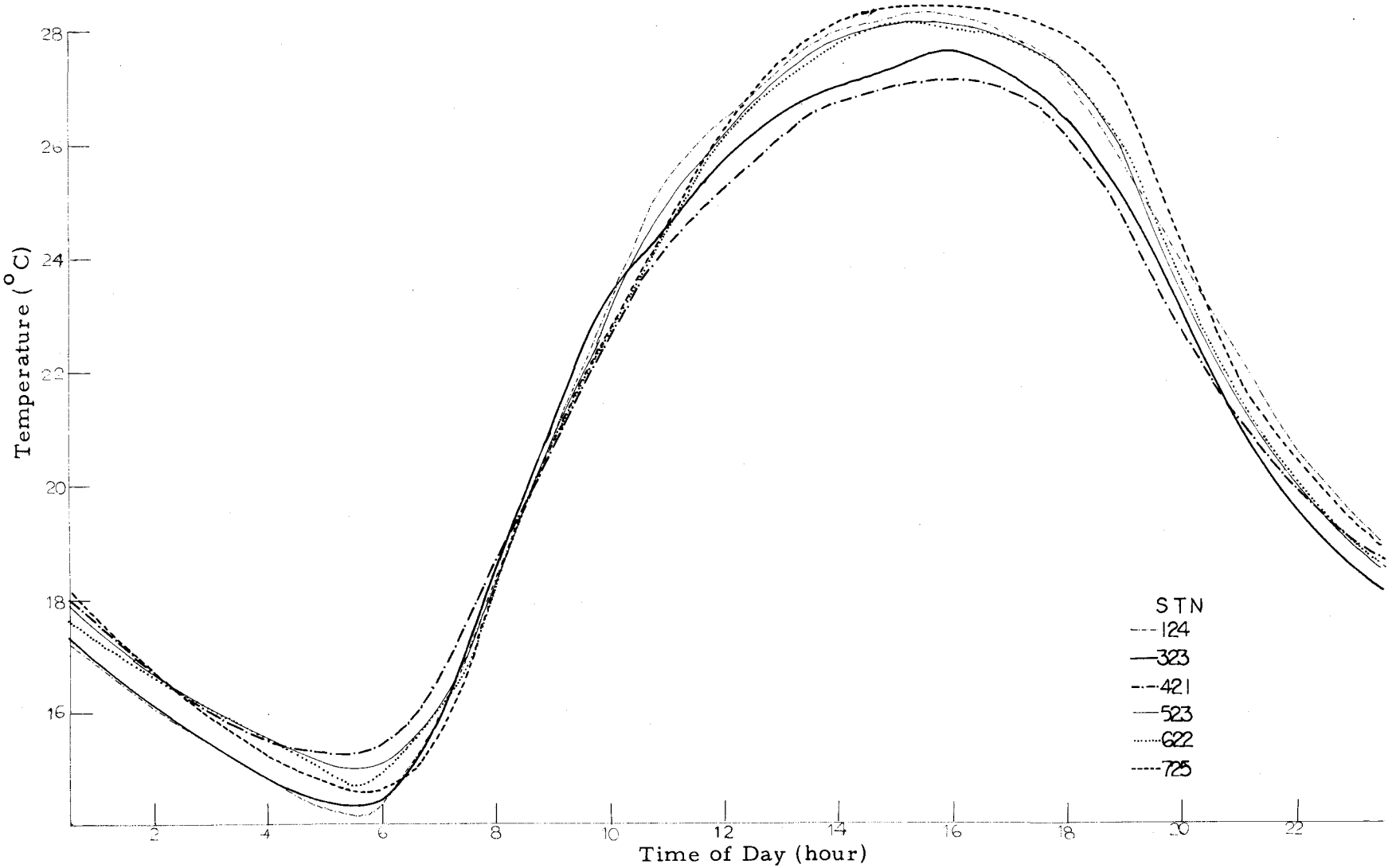

Figure 3. Composite plot of daily distributions of temperature.

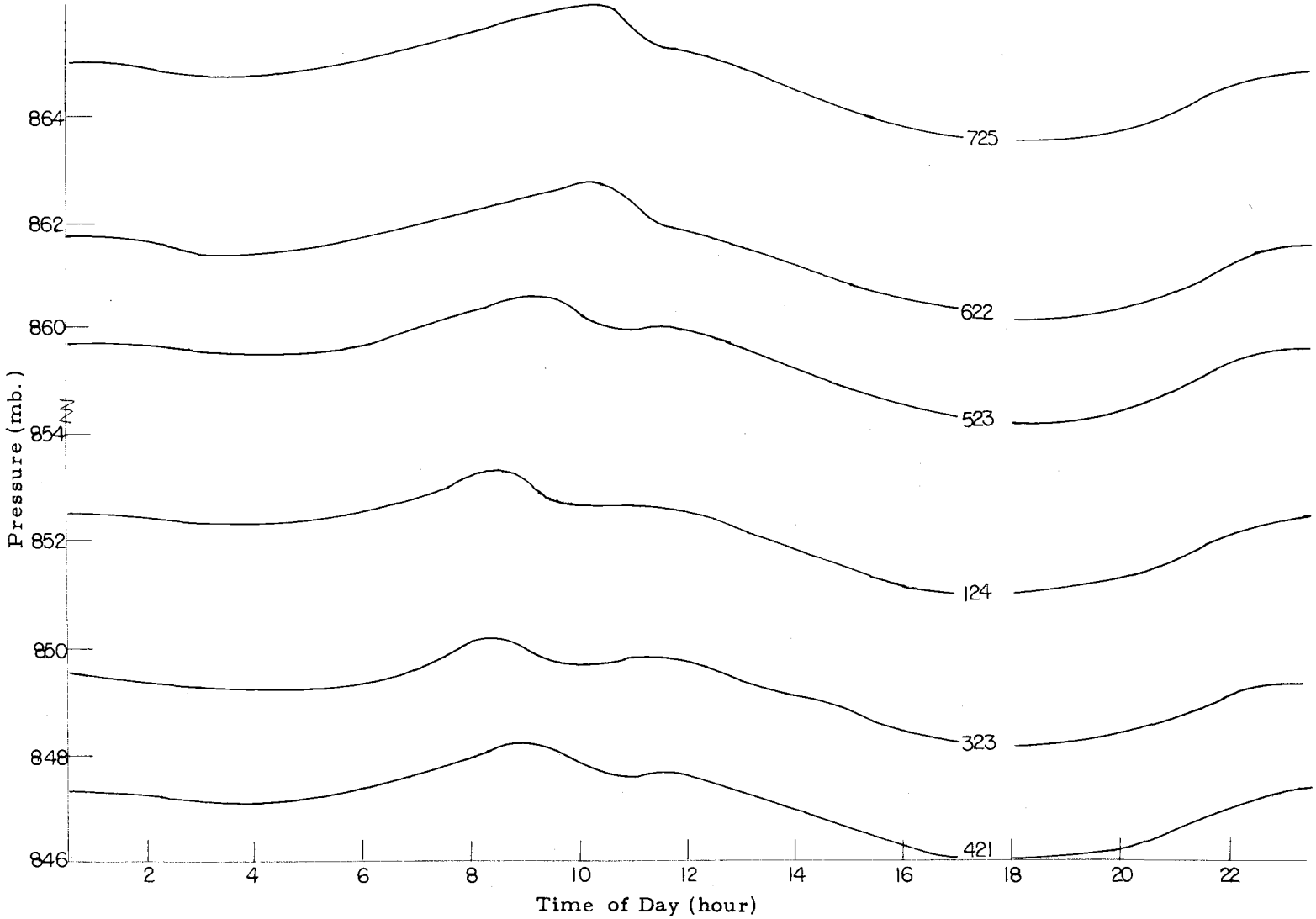

Figure 4. Composite plot of daily distributions of pressure.

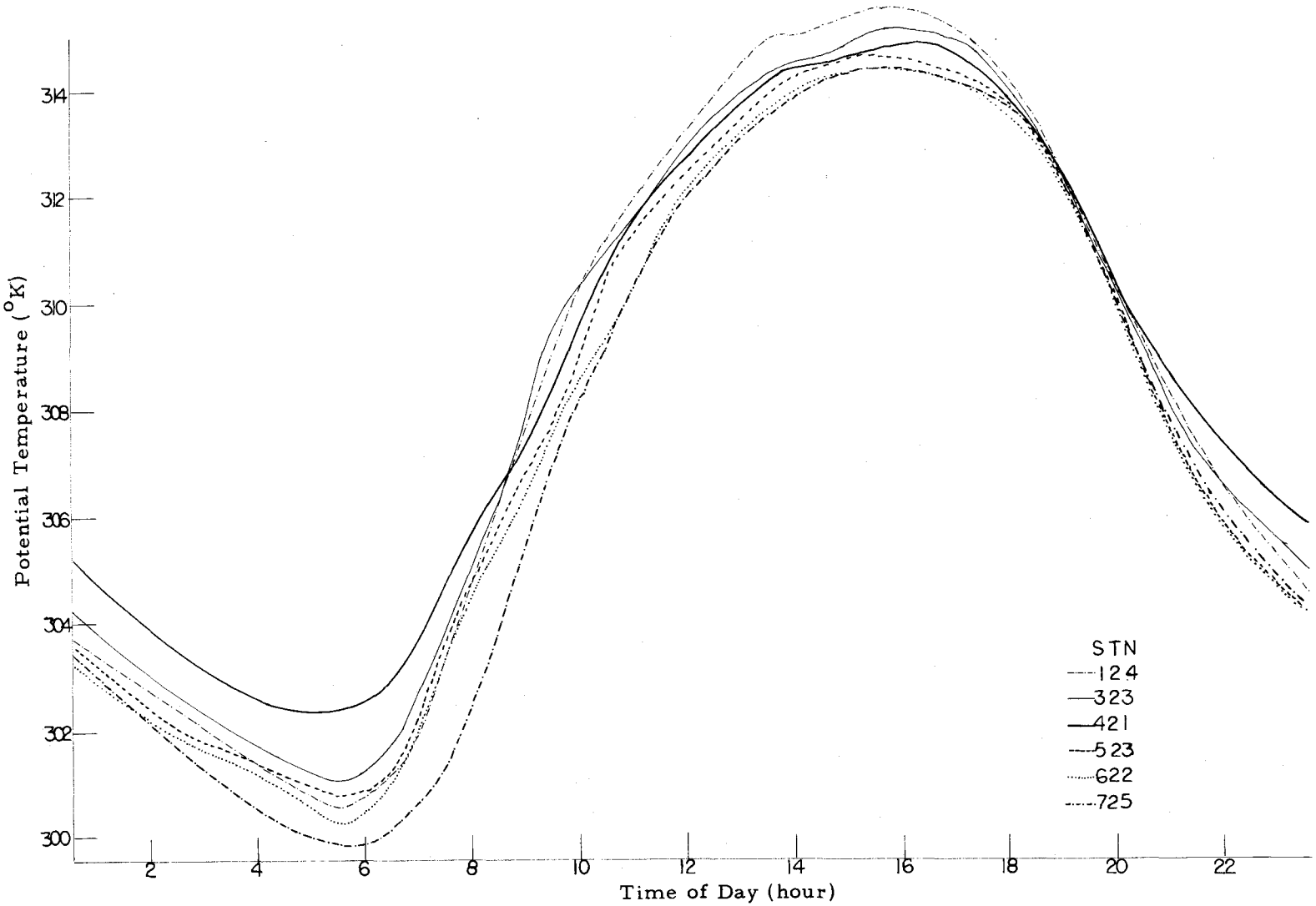

Figure 5. Composite plot of daily distributions of potential temperature.

Figure 3 shows minimum temperature at all stations occurs between 0500 and 0600, just before sunrise. Then temperature climbs rapidly until a maximum is reached at about 1600. A closer look reveals that for stations along the slope (Stations 421, 523, 622, and 725), the lower the elevation, the lower the minimum temperature and the higher the maximum temperature. Similar trends have been observed by Beiger (1957). This is attributed to the fact that in the afternoon, when incoming solar radiation is strong, turbulent effects are important. This turbulent mixing inhibits the prolonged existence of differences in horizontal potential temperature via vertical mixing and upslope flow. At night, outgoing radiation dominates and turbulence is suppressed, so that differences in horizontal potential temperature are not smoothed out.

The average potential temperature at station 421 is almost always higher than the average potential temperature at station 725. This indicates that air above the slope is stable most of the time. The differences in potential temperature between various stations at certain times of the day (0530, 1530, and 2030) are calculated (Tables 6, 7, and 8). From these tables, one finds that at 0530, out of 23 cases, there is not a single case where instability of the order of 1°C exists between station 421 and 725. There are only two such occurrences out of 23 cases each at 1530 and 2030.

Table 6. Differences in potential temperature (°K) at 0530.

Date	Stations A / B	323 / 421	323 / 523	323 / 622	323 / 725	421 / 523	421 / 622	421 / 725	523 / 622	523 / 725	622 / 725
July	1	-1.01	-0.30	-0.52	-0.12	.71	.49	.89	-0.22	.18	.40
	2	-2.62	.43	.73	-0.05	3.04	3.35	2.56	.31	-0.48	-0.79
	3	-2.20	.17	1.98	4.58	2.37	4.16	6.78	1.81	4.41	2.60
	4	-1.55	2.73	2.93	3.98	4.28	4.48	5.52	.20	1.25	1.05
	6	-0.22	.29	2.05	3.47	.51	2.27	3.69	1.76	3.18	1.42
	7	-1.99	.95	.80	2.57	2.93	2.79	4.56	-0.14	1.63	1.77
	8	-0.41	.21	1.03	2.37	.62	1.45	2.78	.83	2.16	1.33
	10	.38	3.70	4.42	3.47	3.32	4.04	3.09	.72	-0.23	-0.95
	11	-0.60	2.11	2.16	-0.13	2.72	2.76	.47	.05	-2.24	-2.29
	12	-1.02	-0.81	-0.77	-0.90	.21	.25	.13	.04	-0.08	-0.13
	13	-0.32	-0.19	.17	-0.04	.13	.50	.28	.37	.15	-0.21
	14	-0.99	.16	.88	.75	1.15	1.67	1.74	.72	.59	-0.13
	15	-1.51	3.06	1.98	1.34	4.57	3.50	2.85	-1.08	-1.72	-0.64
	17	-0.80	-1.30	-1.33	-1.35	-0.50	-0.53	-0.55	-0.04	-0.05	-0.01
	18	.10	1.23	1.06	.45	1.13	.96	.35	-0.18	-0.78	-0.61
	23	-1.41	-1.38	-1.38	-0.73	.02	.02	.67	.00	.65	.65
	24	-0.41	-0.46	-0.52	.58	-0.06	-0.11	.99	-0.06	1.04	1.10
	25	-4.04	-1.31	-1.34	.60	2.73	2.70	4.64	-0.03	1.90	1.94
	26	-1.88	-0.43	.83	1.13	1.45	2.71	3.01	1.26	1.56	.30
	27	-1.56	.13	1.56	2.47	1.69	3.11	4.03	1.42	2.34	.92
	28	-1.00	-0.94	.29	-0.55	.06	1.29	.45	1.23	.39	-0.84
	29	.12	-0.52	.94	1.45	-0.64	.82	1.33	1.46	1.98	.52
	30	-2.15	.96	2.72	3.88	3.11	4.87	6.03	1.76	2.92	1.16
Mean		-1.18	.37	.90	1.27	1.55	2.08	2.45	.53	.90	.37
S.D.		1.02	1.40	1.48	1.75	1.55	1.60	2.09	.78	1.58	1.13

Note: Difference is obtained by subtracting the potential temperature at station B from the potential temperature at station A.

Table 7. Differences in potential temperature (°K) at 1530.

Stations A / Date	B	323 421	323 523	323 622	323 725	421 523	421 622	421 725	523 622	523 725	622 725
July	1	.50	1.63	1.37	1.94	1.13	.87	1.44	-0.26	.31	.57
	2	1.16	1.83	2.99	3.96	.67	1.83	2.80	1.16	2.13	.98
	3	.10	-0.18	.73	1.83	-0.28	.63	1.73	.91	2.01	1.10
	4	-0.28	-0.03	-0.49	.48	.24	-0.21	.76	-0.46	.51	.97
	6	.77	.70	1.50	-0.51	-0.07	.74	-1.28	.80	-1.21	-2.01
	7	.38	.94	1.12	1.14	.55	.74	.75	.19	.20	.01
	8	.78	1.41	1.41	1.71	.72	.72	1.01	.00	.30	.29
	10	.53	.89	1.30	1.61	.36	.77	1.08	.41	.72	.31
	11	.63	.72	1.38	1.43	.09	.75	.79	.66	.71	.05
	12	-0.48	-0.62	-0.03	1.12	-0.14	.45	1.60	.59	1.74	1.15
	13	-0.71	-2.01	-1.95	-2.25	-1.30	-1.24	-1.54	.06	-0.24	-0.30
	14	.40	.66	1.44	1.47	.26	1.04	1.07	.77	.81	.03
	15	.95	-0.34	.23	.66	-1.29	-0.72	-0.29	.57	1.00	.43
	17	.42	.91	.66	.92	.48	.23	.50	-0.25	.02	.27
	18	.42	.53	.86	-0.18	.11	.44	-0.60	.33	-0.71	-1.04
	23	.54	1.10	.80	1.34	.56	.25	.79	-0.30	.24	.54
	24	-0.90	-1.18	-1.18	-1.45	-0.28	-0.28	-0.55	-0.00	-0.27	-0.27
	25	.44	.22	.68	-0.27	-0.23	.24	-0.71	.47	-0.49	-0.96
	26	.43	.47	.60	.83	.05	.17	.40	.12	.35	.23
	27	-0.71	-0.04	-0.08	-0.41	.68	.63	.31	-0.04	-0.37	-0.33
	28	.30	1.26	1.69	-0.44	.96	1.39	-0.74	.43	-1.70	-2.13
	29	.18	.72	1.26	.64	.55	1.09	.46	.54	-0.09	-0.63
	30	.52	1.40	.93	1.75	.78	.31	1.13	-0.46	.35	.82
Mean		.28	.48	.75	.75	.20	.47	.47	.27	.28	.00
S.D.		.54	.92	1.02	1.30	.61	.66	1.04	.45	.92	.89

Note: Difference is obtained by subtracting the potential temperature at station B from the potential temperature at station A.

Table 8. Differences in potential temperature (°K) at 2030.

Date	Stations A / B	323 / 421	323 / 523	323 / 622	323 / 725	421 / 523	421 / 622	421 / 725	523 / 622	523 / 725	622 / 725
July	1	1.06	2.93	2.12	2.58	1.87	1.06	1.52	-0.81	-0.34	.46
	2	.22	1.38	1.18	1.86	1.16	.96	1.64	-0.20	.48	.68
	3	-0.93	.62	-0.54	.84	1.55	.39	1.77	-1.16	.22	1.38
	4	-0.60	.58	1.27	1.51	1.18	1.87	2.11	.69	.93	.24
	6	1.36	3.38	4.28	1.97	2.02	2.92	.61	.90	-1.41	-2.32
	7	-0.31	.75	.85	1.04	1.07	1.16	1.35	.09	.28	.19
	8	-1.81	-0.03	-0.55	.68	1.78	1.26	2.49	-0.52	.71	1.23
	10	.77	1.50	1.98	1.29	.73	1.20	.51	.48	-0.21	-0.69
	11	.66	1.70	.71	-0.50	1.04	.05	-1.16	-0.99	-2.20	-1.21
	12	-0.55	-0.38	.50	.79	.17	1.05	1.34	.88	1.17	.29
	13	-0.50	-1.31	-1.55	-1.95	-0.81	-1.05	-1.45	-0.24	-0.64	-0.40
	14	.25	-0.07	.28	.24	-0.31	.03	-0.01	.35	.30	-0.04
	15	1.30	1.21	.74	1.39	-0.09	-0.57	.09	-0.47	.18	.65
	17	.07	-0.33	-0.03	.09	-0.41	-0.10	.02	.30	.43	.12
	18	.50	1.26	1.50	.54	.76	.99	.04	.24	-0.72	-0.96
	23	-1.76	-0.84	-0.65	-0.51	.92	1.11	1.25	.19	.33	.14
	24	-0.95	-0.56	-0.22	-0.87	.39	.73	.09	.34	-0.31	-0.65
	25	-1.10	.17	.35	-1.45	1.27	1.45	-0.34	.18	-1.61	-1.79
	26	-0.58	-0.15	-0.55	-0.72	.42	.02	-0.14	-0.40	-0.56	-0.16
	27	.54	.53	.33	-0.43	-0.01	-0.21	-0.97	-0.20	-0.96	-0.76
	28	.03	1.58	2.32	.66	1.55	2.28	.63	.74	-0.92	-1.66
	29	-0.44	1.11	.78	-0.03	1.55	1.22	.41	-0.33	-1.14	-0.81
	30	-0.34	.55	.10	.88	.88	.44	1.22	-0.45	.34	.79
Mean		-0.14	.68	.66	.43	.81	.80	.57	-0.02	-0.25	-0.23
S.D.		.88	1.13	1.24	1.13	.78	.92	1.04	.58	.86	.96

Note: Difference is obtained by subtracting the potential temperature at station B from the potential temperature at station A.

The mean and standard deviations of these differences were also computed (Tables 6, 7, and 8). Results of the calculation confirms that the air is always stable along the slope at night and is also stable over 75% of the time during daylight hours during this study period.

If heating along a slope generates a horizontal gradient in potential temperature in such a way that a station at a lower elevation has a higher potential temperature than a station at a higher elevation, local instability along the slope will result. Also, this will lead to a minimum thermodynamic stability if a well mixed layer is assumed. This instability will generate upslope flow and low level convergence at crests that act to support thunderstorm formation. However, the fact that the average difference in horizontal potential temperature along the slope is small in the afternoon and is positive (stable) over 75% of the time suggests that thunderstorms resulting from terrain induced local instability over the NHRE network may be uncommon.

Daytime differences in horizontal potential temperature and thus baroclinicity appear to be important only during late morning and early afternoon. Here I assumed a well mixed layer so that gradients in horizontal potential temperature can be inferred by potential temperatures along the slope. However, resulting circulations transport heat, thus reducing the gradient in horizontal potential temperature. Thus, by mid and late afternoon, when hail activity is at a statistical

maximum, horizontal potential temperature differences are at a minimum (Figure 5).

The positive gradient in upslope potential temperature at night indicates that the downslope flow is thermodynamically stable, especially after midnight. This implies that the downslope flow is driven by baroclinicity and strongly influenced by friction.

B. Wind Analysis

Twenty-one days of good data in the month of July were used in the analysis of the diurnal variation in the wind structure at station 622 (Table 9). Hourly averages of wind speed and direction were obtained from microfilms of strip charts. Data accuracy is subjectively considered to be about ± 5° and ± 0.2 m/s. Wind direction and speed are then decomposed into u, v components, where u is positive for winds coming from the west and negative for winds coming from the east. The component v is positive for northerly flow and negative for southerly flow, and is thus roughly parallel to the line of stations under investigation, which, as mentioned before, are along a straight line running from north to south. The u, v components for each hour are then averaged over the 21 day period (Table 10). In this manner, the influence on wind direction and speed due to synoptic scale disturbances is reduced.

Table 9. Days when wind data are reliable.

	S	M	T	W	T	F	S
July		2	3	4		6	7
	8		10	11	12	13	14
	15		17	18			
		23	24		26	27	28
	29	30					

Table 10. Monthly mean wind components.

Time (hr)	u (m/s)	v (m/s)
00	-0.21	-1.18
01	0.47	-1.07
02	0.75	-1.34
03	0.52	-1.83
04	0.46	-1.94
05	0.42	-1.96
06	0.27	-1.49
07	-0.29	-1.44
08	-0.58	-1.33
09	-1.06	-0.98
10	-1.64	-0.47
11	-1.47	-0.05
12	-1.53	0.24
13	-1.45	0.82
14	-0.78	0.87
15	-1.53	0.34
16	-1.46	0.49
17	-1.30	0.91
18	-1.23	0.90
19	-1.32	-0.11
20	-0.83	0.09
21	0.10	-0.40
22	0.16	-0.62
23	-0.06	-0.18

A hodograph (Figure 6), drawn from the calculated mean u, v components for the 21 days shows that, starting from midnight, the surface wind backs until 0200 and then veers until 1400. A maximum wind is obtained at 0500 and 1700. After 1400, the wind can be seen to undergo two more directional oscillations before coming back to its starting position at midnight. From noon till 1800, the wind blows generally from the southeast and at night, from midnight till 0600 the wind is generally from the northwest. Thus, an upslope wind occurs during the afternoon and a downslope wind at night.

To obtain a better picture of the averaged wind changes, days with sudden rise of wind speed of more than 5 m/s in one hour are discarded from the 21 days, leaving 15 days which are free of synoptic disturbances and thunderstorms (Table 11). The mean value of u, v components for the 15 days was computed (Table 12) and a hodograph drawn (Figure 7).

Careful scrutiny of the wind vectors shows again, from 0900 to 2000, the wind is coming from the southeast and during the night, from 0100 to 0600, the wind is from the northwest. However, in this hodograph, which should have a lesser influence by synoptic disturbances, four oscillations are distinctly discernable. The first one is from approximately 2330 to 0800. The second one is from 1000 to 1400, the third one from 1430 to 1900 and the fourth one from 2030 to 2330. At any rate, the flow is again predominently along the slope.

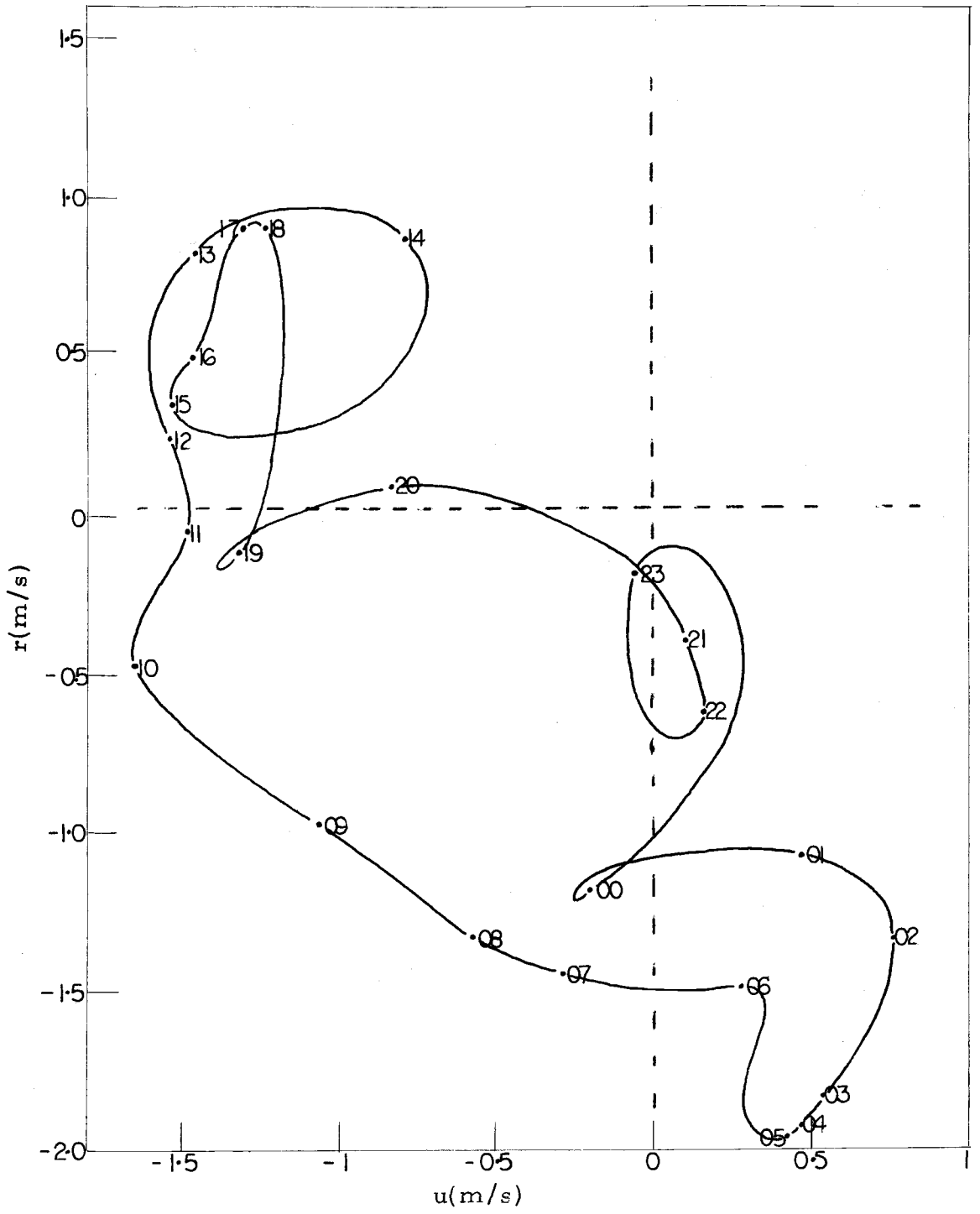

Figure 6. Hodograph of Monthly Mean Wind Velocity.

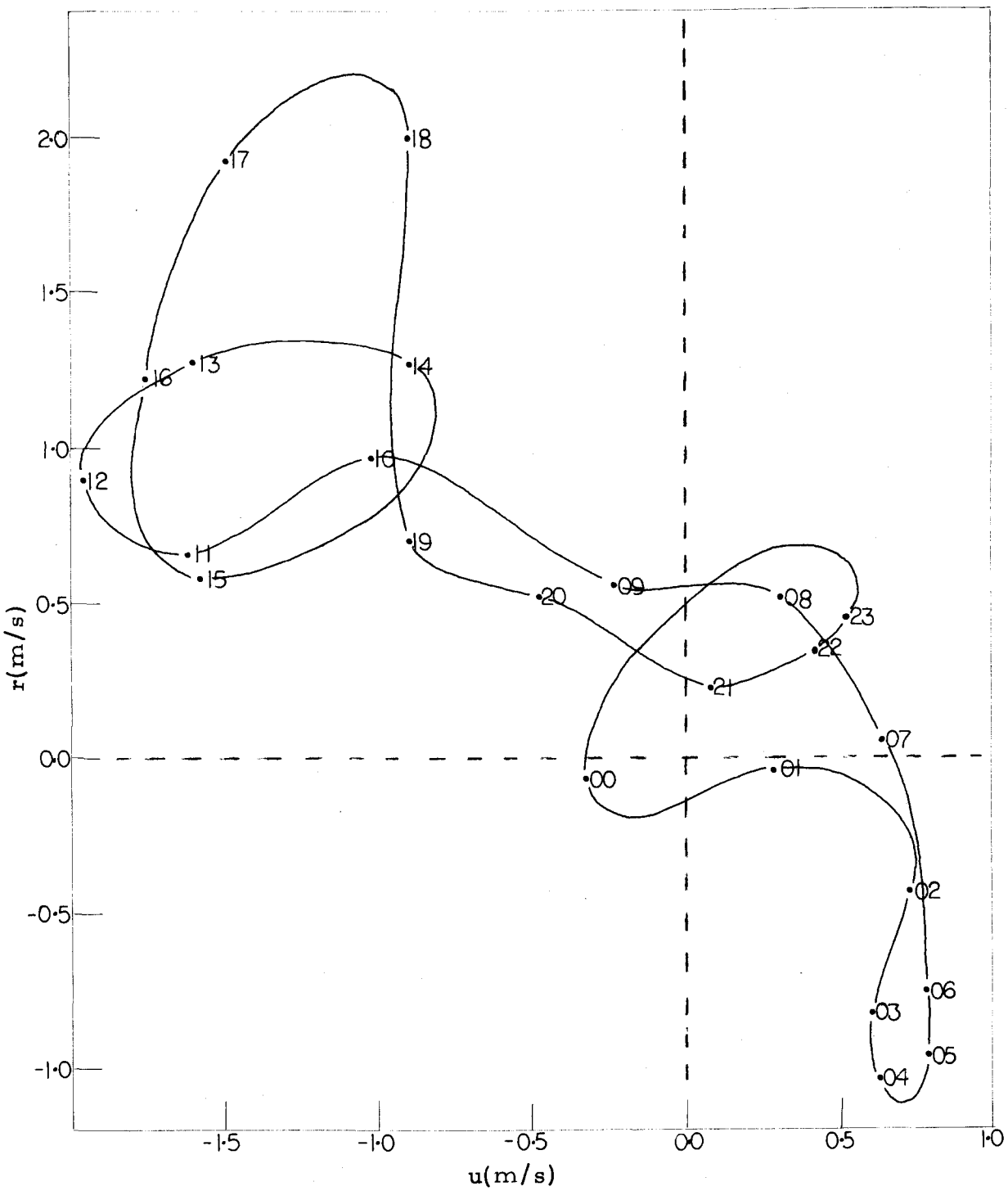

Figure 7. Hodograph of Selected Mean Wind Velocity.

Table 11. Selected days of wind data.

	S	M	T	W	T	F	S
July		2	3	4			7
	8		10	11			14
	15			18			
			24		26	27	28
		30					

Table 12. Selected mean wind components.

Time (hr)	u (m/s)	v (m/s)
00	-0.32	-0.07
01	.28	-0.04
02	.72	-0.44
03	.61	-0.83
04	.63	-1.05
05	.79	-0.97
06	.78	-0.78
07	.63	.05
08	.33	.51
09	-0.23	.55
10	-1.02	.97
11	-1.61	.66
12	-1.95	.90
13	-1.59	1.28
14	-0.89	1.27
15	-1.57	.58
16	-1.75	1.22
17	-1.49	1.93
18	-0.89	2.01
19	-0.90	.70
20	-0.47	.52
21	.09	.23
22	.42	.34
23	.52	.45

The maximum speed in the day time is at 1700 and the maximum night time speed is at 0500.

Both hodographs show that air moves upslope during the day time until a maximum is reached at 1700 and then air moves downslope at night until a maximum speed is reached at 0500, just before the sun rises. This suggests that the air circulation along a slope can be associated with baroclinicity due to diurnal heating along the slope. When horizontal accelerations are large, (there does not exist a balance between "friction," horizontal pressure gradient and Cariolis terms where "friction" refers to the divergence of turbulence momentum flux), the flow will tend toward low pressure (upslope in the daytime, downslope at night). Possible causes for sub-diurnal wind oscillations are listed in Section VIII.

C. Thermal Wind

In this section, an order of magnitude estimate of the diurnal variation of the wind is attempted by employing geostrophic relationships. The fundamental equations used are the geostrophic wind equation, the hydrostatic equation, the equation of state and Poisson's equation. These respective equations are:

$$fu = -\frac{1}{\rho}\frac{\partial p}{\partial y}$$

$$\frac{\partial p}{\partial z} = -\rho g$$

$$p = \rho R T$$

$$\frac{T}{\theta} = \left(\frac{p}{p_0}\right)^{R/C_p}$$

where

u horizontal velocity

f Coriolis parameter

ρ density

p pressure

y horizontal coordinate

R gas constant

g gravitational force

z vertical coordinate

T temperature

θ potential temperature

p_0 standard pressure (1000 mb)

$R/C_c = 0.286$

The thermal wind equation obtained from these equations has the following form:

$$f\frac{\partial u}{\partial z} = -\frac{g}{\theta}\frac{\partial \theta}{\partial y} + \frac{fu}{\theta}\frac{\partial \theta}{\partial z}$$

The first term in the right of the equation is approximately $9.8 \frac{1}{\theta} \frac{\partial \theta}{\partial y}$ and the second term $\frac{3 \times 10^{-4}}{\theta} \frac{\partial \theta}{\partial z} \frac{1}{\theta}$. It is difficult to compare $\frac{\partial \theta}{\partial y}$ and $\frac{\partial \theta}{\partial z}$ because the flow structure perpendicular to the slope is not known. But, even if $\frac{\partial \theta}{\partial z}$ is one or two orders of magnitude greater than $\frac{\partial \theta}{\partial y}$, the first term still dominates. Consequently, $f \frac{\partial u}{\partial z}$ is approximated by $- \frac{g}{\theta} \frac{\partial \theta}{\partial y}$ or $- \frac{g}{\theta} \frac{\Delta \theta}{\Delta y}$, and u_T by $- \frac{g}{f\theta} \frac{\partial \theta}{\partial y} \Delta z$ or $- \frac{g}{f\theta} \frac{\Delta \theta}{\Delta y} \Delta z$.

At 0500 and 1700, the observed wind speeds were at a maximum (see Section V). The thermal wind is approximated using observed data at station 421 and station 725. Δy is 27.5 km and Δz is 150 m (Table 1). At 0500 θ at station 421 is 302.3°K and at station 725, 299.8°K (Table 5). The magnitude of the thermal wind is thus found to be 4.45 m/s. Similarly, the magnitude of the thermal wind at 1700 is approximately 0.51 m/s.

This simple calculation suggests that thermal wind effects are more important in the pre-dawn period than in the afternoon. That the observed upslope flow is stronger than downslope flow may be due to synoptic influences, accelerations and diurnal variations of thermodynamic stability.

Holton (1967) finds that at 0600, the thermal wind above the Great Plains for neutral stability is 5 m/s, and at 1800, the thermal wind is 2 m/s. His calculation is based on a much larger spatial scale.

My calculation indicates that the thermal wind effect in the morning is an order of magnitude greater than in the afternoon. This further substantiates my previous conclusion that in the afternoon, thermally (baroclinically) driven circulation in the NHRE mesoscale is not conspicuous, and resulting mass convergence near terrain crests appears not to be an important cause for thunderstorm initiation. One must, however, acknowledge the complication that the observed winds reflect diurnally varying thermal winds on two different scales of motion.

D. Harmonic Analysis

In order to determine the distribution of energy in the wind system, a harmonic analysis was performed on the mean wind speed at station 622. Twenty-four hourly wind speeds were obtained by averaging data at each hour over a period of 21 days (hereinafter called monthly mean) as well as over a period of 15 days (hereinafter called selected mean) (Table 13). Hodographs for these two daily distributions obtained by averaging over different time period have been presented in the section on Wind Analysis.

Table 13. Daily distribution of hourly wind speeds.

Time of day (hr)	Monthly Mean (m/s)	Selected mean (m/s)
00	1.20	0.33
01	1.17	0.28
02	1.54	0.84
03	1.90	1.03
04	1.99	1.22
05	2.00	1.25
06	1.51	1.10
07	1.47	0.63
08	1.45	0.61
09	1.44	0.60
10	1.71	1.41
11	1.47	1.74
12	1.55	2.15
13	1.67	2.04
14	1.17	1.55
15	1.57	1.67
16	1.54	2.13
17	1.59	2.44
18	1.52	2.20
19	1.32	1.14
20	0.83	0.70
21	0.41	0.25
22	0.64	0.54
23	0.19	0.69

According to mathematical principles, any function which is given at every point in the interval can be represented by a Fourier Series:

$$f(x) \sim \frac{1}{2} a_0 + \sum_{n=1}^{\infty} (a_n \cos nx + b_n \sin nx)$$

where a_0, a_n, and b_n are Fourier coefficients. Now, if only a

finite number of points exist in the interval to be analyzed, a finite number of sines and cosines will be able to account for all the observations. In one day, there are 24 hourly mean wind speed readings so that 11 sine terms and 12 cosine terms will be sufficient to describe the diurnal variation completely. It is this determination of a finite sine and cosine series that is called "harmonic analysis." The series representing the averaged daily wind variation is as follows:

$$X(t) = \overline{X} + \sum_{i=1}^{12} [A_i \sin(\frac{360^\circ}{P} it) + B_i \cos(\frac{360^\circ}{P} it)]$$

where $\overline{X}$ is the daily average and P, the fundamental period, which in this case is 24 hours. A_i and B_i are the coefficients with $A_{12} = 0$. The following formulas provide a means of finding the various coefficients:

$$A_i = \frac{2}{N} \sum [X \sin(\frac{360^\circ}{P} it)]$$

$$B_i = \frac{2}{N} \sum [X \cos(\frac{360^\circ}{P} it)]$$

where N is the total number of observations or data points. The summation in these formulas extends over the 24 observations. It is

for finding the amplitude of the ith harmonic (C_i) that A_i's and B_i's are computed.

$$C_i \cos[\frac{360°}{P} i(t-T_i)] = A_i \sin(\frac{360°}{P} it) + B_i \cos(\frac{360°}{P} it)$$

and

$$C_i = \sqrt{A_i^2+B_i^2}, \quad T_i = \frac{P}{2\pi i} \arctan \frac{A_i}{B_i}$$

where T_i is the time at which the ith harmonic has a maximum. The variance accounted for by a harmonic is $C_i^2/2s^2$ where s^2 is the total variance given as

$$s^2 = \frac{\Sigma X^2}{N} - (\bar{X})^2$$

The coefficients A_i and B_i will be the same regardless of the origin of X. The origin of time is also immaterial. Changing the time origin will change A_i and B_i but will not affect the amplitude of C_i. In this analysis, t = 1 at time = 0000 and t = 2 at time = 0100, etc.

The results of the analysis of monthly mean speeds are given in Table 14. The results show that $C_1 = C_2 = 0.38$ and $C_3 = 0.23$. The variance for the respective harmonics are 36%, 36% and 13%. $T_1 = 9.89$, $T_2 = 5.00$ and $T_3 = 3.53$. The sum of these first three variances is 85%. This indicates that 85% of the wind's energy is

represented by C_1, C_2, and C_3.

Table 14. Harmonic analysis of monthly mean wind speeds.

i	A_i (m/s)	B_i (m/s)	C_i (m/s)	Variance	T_i (hr)
1	0.20	-0.33	0.38	0.36	9.89
2	0.19	-0.33	0.38	0.36	5.00
3	0.08	-0.22	0.23	0.13	3.53
4	0.02	0.05	0.05	0.01	0.27
5	0.03	0.03	0.04	0.00	0.58
6	0.04	-0.03	0.05	0.01	1.59
7	-0.01	-0.01	0.02	0.00	2.20
8	-0.03	-0.09	0.09	0.02	1.66
9	0.06	-0.03	0.07	0.01	0.82
10	-0.05	-0.12	0.13	0.04	1.34
11	0.02	-0.09	0.09	0.02	1.02
12	0.00	-0.04	0.04	0.01	0.00

The results of the analysis of selected wind speeds are given in Table 15. $C_1 = 0.68$, $C_2 = 0.43$. The variances of these two harmonics sum up to 75%. The first harmonic has a time of maximum at 14.86 hours while the second has a time of maximum at 4.48 hours. These harmonics indicate the importance of diurnal and semi-diurnal oscillations. The first harmonic resulting from analyzing selected wind speeds has a time maximum at approximately 1500 when the stability is at a minimum, and at which time mixing of higher momentum from aloft is at a maximum. Semi-diurnal oscillations with downslope maximum at 0500 and upslope maximum at 1700 have already been seen to occur from wind analyses discussed in Section V.

Table 15. Harmonic analysis of selected mean wind speeds.

i	A_i (m/s)	B_i (m/s)	C_i (m/s)	Variance	T_i (hr)
1	-0.47	-0.49	0.68	0.54	14.86
2	0.29	-0.32	0.43	0.21	4.48
3	-0.00	-0.21	0.21	0.05	4.01
4	0.07	0.35	0.35	0.14	0.20
5	-0.15	0.05	0.16	0.03	3.86
6	-0.04	0.00	0.04	0.00	3.00
7	0.00	0.07	0.07	0.01	0.01
8	-0.00	0.04	0.04	0.00	2.95
9	0.03	0.06	0.07	0.01	0.23
10	-0.06	0.00	0.06	0.00	1.80
11	0.01	0.00	0.01	0.00	0.44
12	0.00	-0.08	0.08	0.01	0.00

E. Power Spectrum Analysis

The longest available continuous time series of wind velocity for station 622 and station 421 is further analyzed. This time series begins at 1100 on July 10, 1973 and ends at 1000 on July 19, 1973. Hourly mean velocities are used (Tables 16, 17); there are 216 discrete data points, 24 data points for each of the nine days. This is really too short to be statistically significant. However, a comparison between spectra at two stations may yield useful information.

As a first step, autocorrelation coefficients for each time series are separately calculated using the formula:

$$r_L = \frac{\sum_i (X_i - \overline{X})(X_{i+L} - \overline{X})}{S_x^2 N} \qquad (1)$$

Table 16. Time series of wind speeds (m/s) at station 622.

Time (hr)	July									
	10	11	12	13	14	15	16	17	18	19
00	-	3.2	4.0	8.8	3.5	1.7	0.1	2.7	2.3	4.5
01	-	3.3	2.9	9.0	2.8	1.7	0.1	2.3	2.6	5.1
02	-	3.9	2.3	10.3	2.3	1.9	0.2	2.0	4.3	4.4
03	-	4.0	1.7	10.4	2.4	1.2	0.2	1.6	5.4	4.2
04	-	3.4	1.4	10.6	2.4	1.4	0.2	1.4	4.9	4.6
05	-	3.0	1.7	9.3	3.6	1.1	0.3	1.5	7.1	5.7
06	-	2.3	1.9	8.9	2.7	1.5	0.3	1.8	8.4	5.0
07	-	4.1	1.8	10.0	3.3	1.8	0.4	2.3	10.3	6.2
08	-	6.5	1.1	10.9	3.7	3.3	0.4	1.4	9.4	6.4
09	-	7.5	2.8	8.6	3.8	4.5	0.3	1.6	8.3	6.6
10	-	7.7	3.2	9.3	3.6	4.4	0.1	1.7	7.0	6.7
11	2.3	7.8	1.9	9.6	4.3	4.7	0.1	2.3	7.0	-
12	2.9	7.8	1.8	9.9	4.3	4.1	0.6	2.7	6.7	-
13	3.5	7.1	2.4	9.1	3.7	2.8	3.0	3.7	4.4	-
14	3.2	6.2	1.7	9.9	3.3	2.5	2.8	3.7	2.3	-
15	3.0	6.7	3.4	11.1	2.4	1.7	3.1	3.4	2.9	-
16	2.7	7.4	5.7	12.4	2.7	1.7	3.3	3.7	3.0	-
17	3.7	6.2	7.4	11.5	2.9	2.3	3.5	2.9	4.2	-
18	3.8	5.4	7.8	10.3	3.1	2.6	4.8	1.9	4.9	-
19	2.9	4.8	6.4	8.0	2.4	1.4	3.9	5.0	5.0	-
20	2.4	3.8	4.8	6.2	2.2	0.4	2.8	3.9	4.0	-
21	2.4	3.0	6.3	4.7	1.8	0.3	2.9	2.8	4.3	-
22	3.1	2.1	7.5	4.4	1.8	0.2	2.8	3.3	3.8	-
23	2.7	3.4	8.9	3.5	1.4	0.1	2.7	1.9	4.0	-

Table 17. Time series of wind speeds (m/s) at station 421.

Time (hr)	July									
	10	11	12	13	14	15	16	17	18	19
00	-	5.8	6.1	8.9	2.8	2.9	4.7	3.4	2.4	3.9
01	-	6.5	5.0	9.8	2.7	2.5	4.0	2.9	3.9	4.3
02	-	6.4	4.4	10.2	2.7	2.5	4.4	3.4	4.2	4.5
03	-	6.4	3.9	10.0	3.0	2.3	4.5	3.4	4.4	4.6
04	-	6.0	3.4	8.5	4.0	2.2	2.5	3.4	6.4	4.4
05	-	5.7	3.4	7.6	3.7	2.1	2.8	2.5	8.9	5.5
06	-	5.9	2.9	7.2	3.4	2.4	3.1	3.9	10.5	5.0
07	-	7.0	4.2	8.6	3.3	3.4	3.5	3.1	11.5	6.0
08	-	8.4	5.8	9.5	3.6	4.4	3.4	2.7	10.2	6.2
09	-	10.0	5.2	7.6	3.7	6.5	2.3	2.2	8.9	5.9
10	-	9.8	3.8	7.4	3.9	7.0	2.7	2.2	7.9	6.4
11	3.1	9.6	3.0	8.4	4.5	6.6	2.8	4.0	7.7	-
12	4.0	9.6	2.7	7.5	5.6	6.2	2.4	5.0	7.0	-
13	4.3	9.0	3.9	7.8	4.0	4.4	3.2	4.0	5.5	-
14	4.4	8.3	4.5	7.8	4.0	3.0	3.2	4.4	2.4	-
15	3.9	6.9	6.5	8.5	4.1	2.4	2.3	4.1	2.9	-
16	3.8	7.2	7.3	11.5	4.1	2.9	2.6	4.1	2.9	-
17	3.9	6.5	7.5	11.4	4.1	1.8	3.9	3.0	4.0	-
18	4.0	6.5	7.7	9.9	3.7	2.2	4.5	5.0	4.3	-
19	4.3	5.8	7.7	6.5	3.5	3.0	5.9	6.0	4.1	-
20	3.3	4.9	5.9	4.7	2.8	3.9	4.0	2.9	4.0	-
21	4.3	5.4	7.6	3.4	2.9	3.3	3.5	2.9	4.2	-
22	5.0	5.3	8.5	3.0	3.0	3.1	3.8	2.8	4.3	-
23	5.3	6.1	9.8	3.7	3.0	3.2	3.3	1.9	4.4	-

where L is the time lag; r_L is the autocorrelation coefficients, X_i is the wind velocity at point i; $\overline{X}$ is the mean wind velocity for the said period; S_x^2 is the total variance; and N is the number of data points.

Autocorrelation coefficients are plotted over the lag hours in Figures 8 and 9. Lags of up to 175 hours are plotted for both stations. Striking similarities are evident in these two graphs. Both curves demonstrate a positive autocorrelation for lags up to 24 hours. This is probably related to diurnal variations. Both curves indicate a negative autocorrelation between lags of approximately 50 to 110 hours, or between two and four-and-half days. This is probably due to synoptic variations.

Using these autocorrelation coefficients, the power spectra for the two time series of wind velocities were calculated. The harmonics are given by

$$B_i = \frac{r_0}{m} + \frac{2}{m} \sum_{L=1}^{m-1} [r_L \cos(\frac{2\pi}{2m} iL) + \frac{r_m}{m} (-1)^i \qquad (2)$$

where r_L is the autocorrelation coefficient for lag L; and m is the longest lag, namely 215 hours in this case. Thus, the fundamental period is $2m$ hours or approximately 18 days, that of the second harmonic m hours, that of the third harmonic $2m/3$ hours, and so forth.

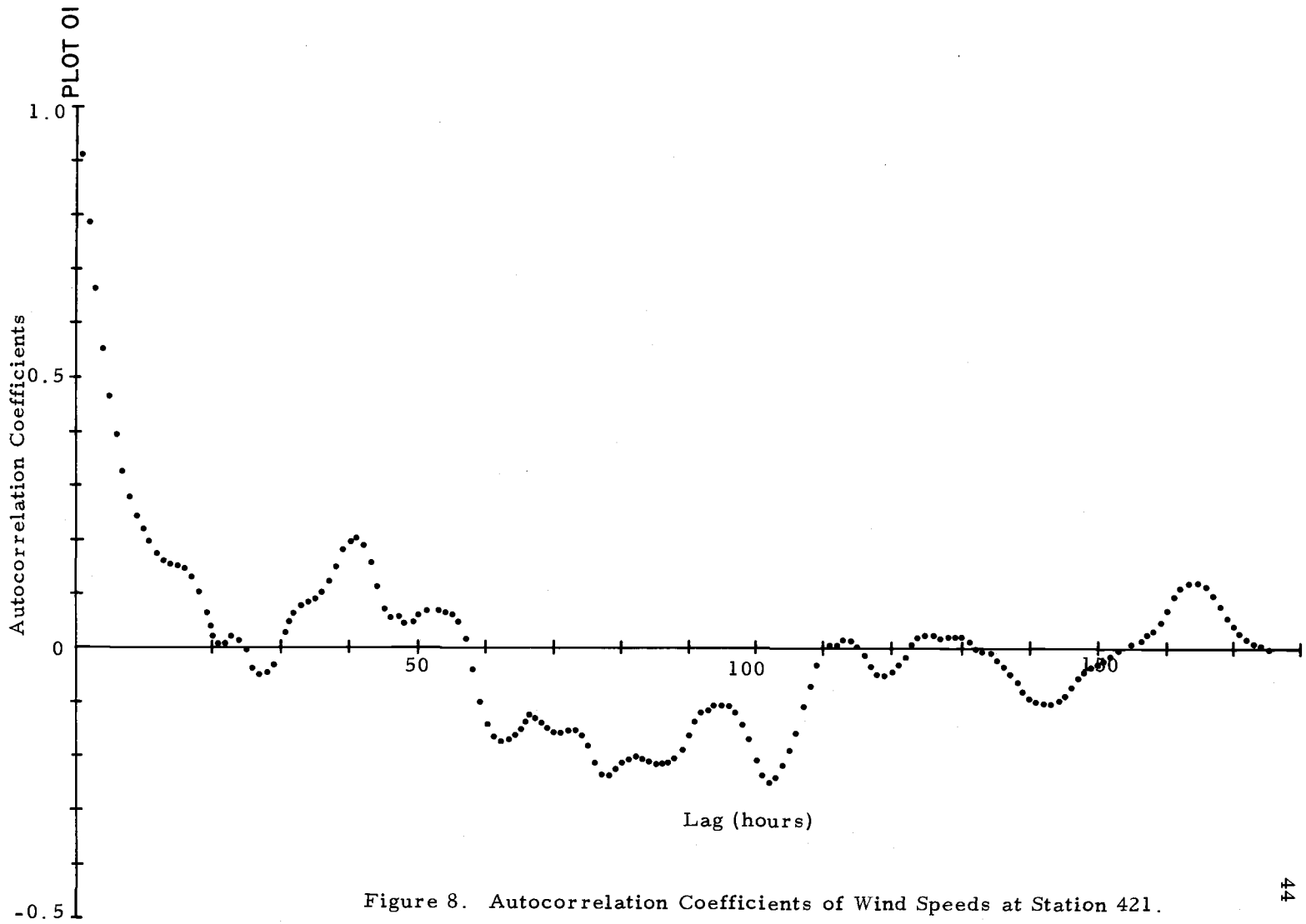

Figure 8. Autocorrelation Coefficients of Wind Speeds at Station 421.

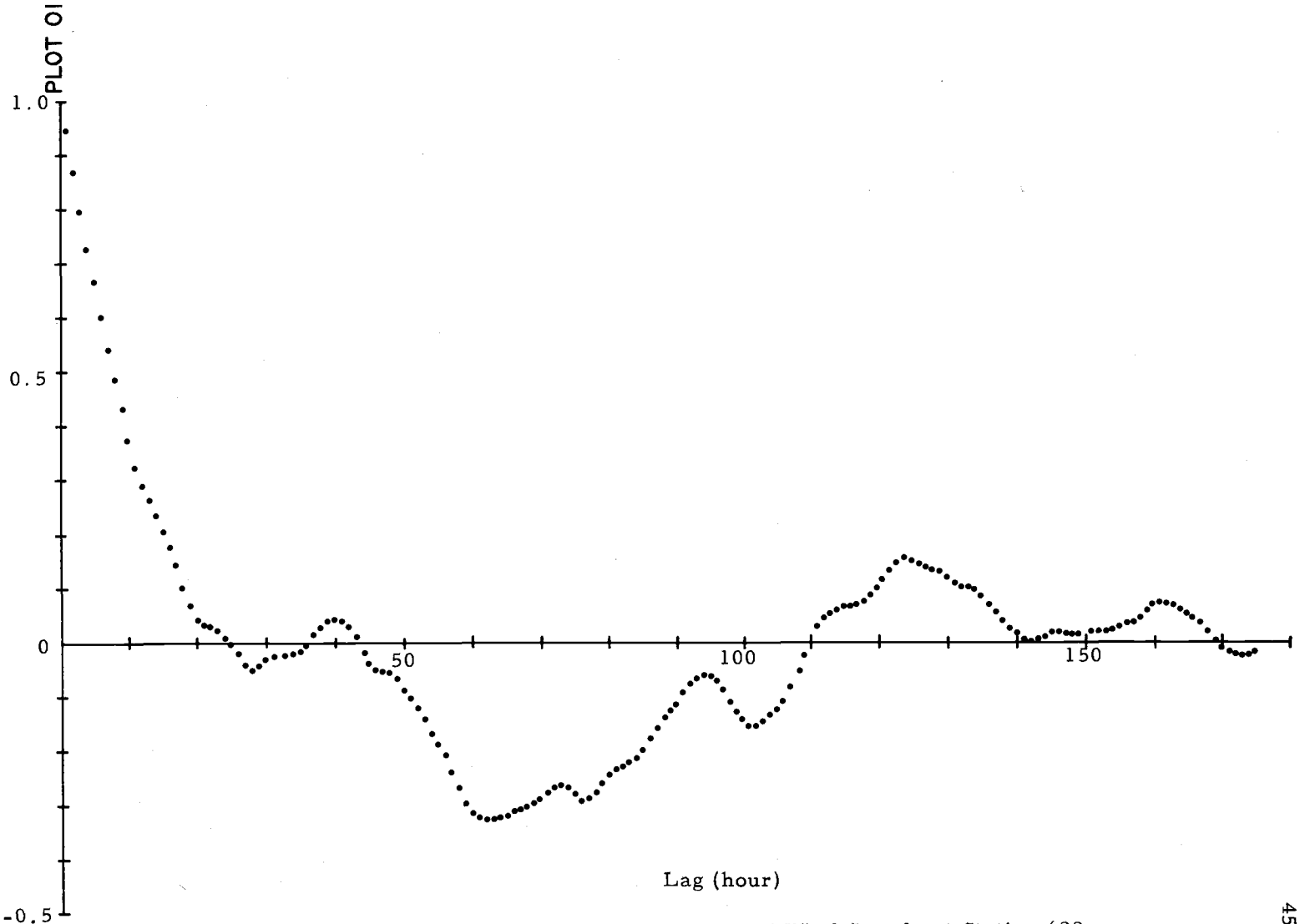

Figure 9. Autocorrelation Coefficients of Wind Speeds at Station 622.

In the case of B_0 and B_m, the coefficients resulting from the formula have to be divided by 2. This formula, however, does not give the best estimates of the smoothed spectrum function because it can give negative weights to the harmonics, resulting in greatly distorted spectral estimates whenever there are rapid fluctuations in the true spectrum. Smoothing of the spectrum can be done using the Blackman-Tukey method (1958):

$$S_i = 0.25B_{i-1} + 0.50B_i + 0.25B_{i+1} \qquad (3)$$

In effect, the coefficients are smoothed by a weighted moving average.

The smoothed spectrum is plotted as a function of frequency ($1/2m\Delta t$, where Δt is one hour). As depicted by Figures 10 and 11, both curves peak at the same or nearly the same frequencies. For station 622, the power spectrum peaks at 3, 10, 19, 23, 32, 42 and 53 cycles/2m hours; and for station 421, it peaks at 2, 8, 19, 23, 31, 40 and 53 cycles/2m hours. The periods for such peaks at station 622 are 143.3, 43, 22.6, 18.7, 13.4, 10.2 and 8.1 hours. The periods for peaks at station 421 are 215, 53.7, 22.6, 18.7, 13.9, 10.7 and 8.1 hours.

Both stations have spectral peaks having periods of 14, 10.5 and 8 hours. These peaks may be related to the structure of the hodographs presented in the section on wind analysis. Insufficient

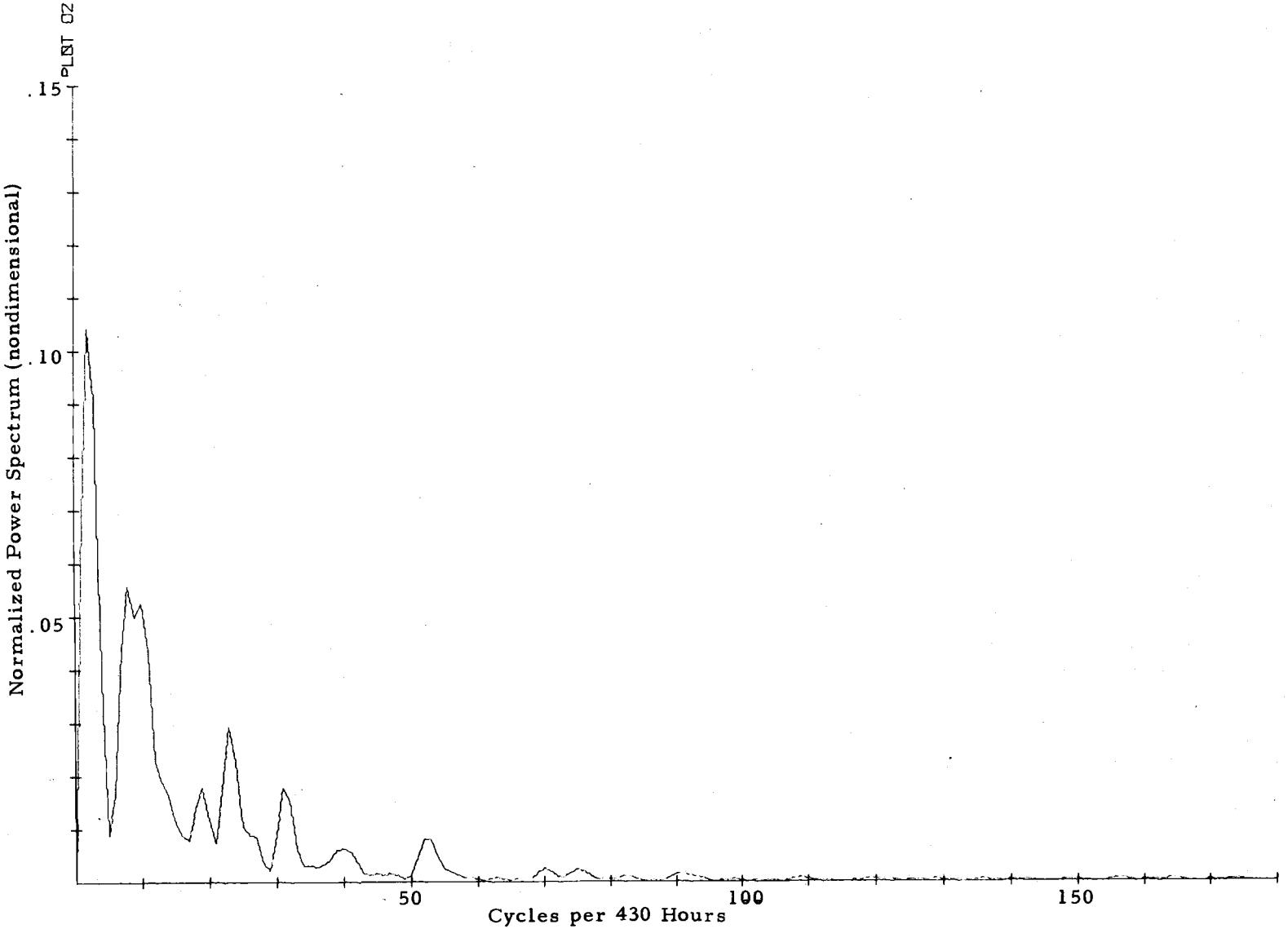

Figure 10. Power Spectrum of Wind Speeds at Station 421.

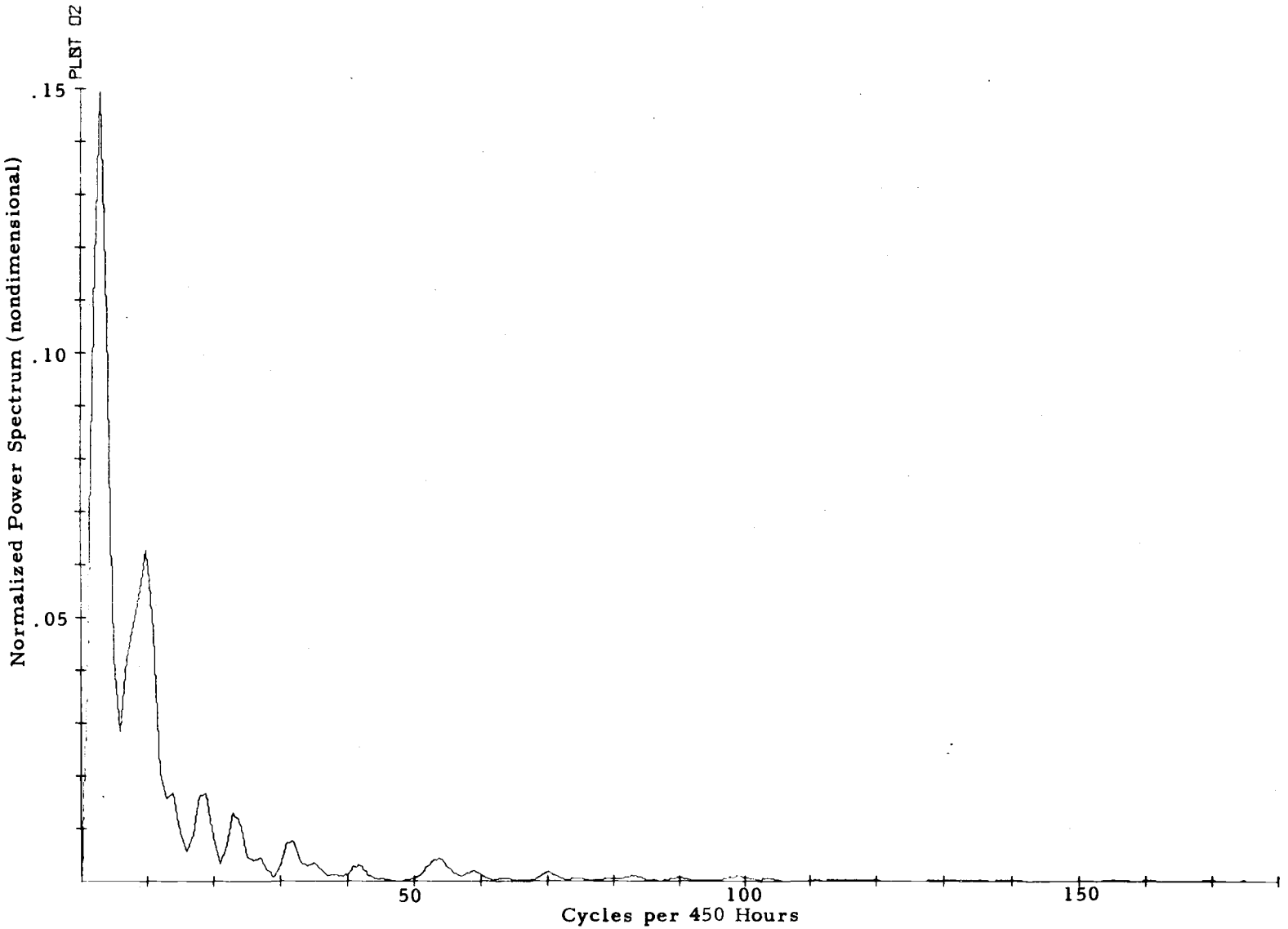

Figure 11. Power Spectrum of Wind Speeds at Station 662.

data (216 points) has made defining the cause behind these peaks rather difficult. Furthermore, from sampling theory alone, peaks and valleys of this sort can be expected to appear in any spectrum constructed from a finite amount of data.

Confidence intervals for each peak can be computed based on a Chi-square distribution. A harmonic that is smoothed using the weighted moving average technique has two degrees of freedom. According to Blackman and Tukey (1958), and 80% confidence interval for an observed estimate of x m^2/s^2 with two degrees of freedom, extends from $x/2.3$ m^2/s^2 to $x/0.1$ m^2/s^2. Thus, the first peak of the power spectrum at station 421 with a value of 0.104 can lie anywhere between 0.045 and 1.040 to give one a confidence of 80%. This greatly reduces the significance of the peak. Similar confidence intervals can be computed for the other peaks with the result that their significance is also reduced. However, since peaks occur at the same frequencies at both stations, speculations as to their physical origin are not unwarranted. Some likely causes are listed below:

1) Superposition of thermal winds due to 50 km scale and 1000 km scale slopes.

2) Gravity inertial waves.

3) Slowly moving quasi-standing waves shed from the Rockies.

Further research will be necessary to determine whether these peaks are due to insufficient data points or are results of one or a

combination of the above speculations.

The peaks having a period of 22.6 hours for both stations suggest the diurnal oscillation of wind strength. The period for an inertial oscillation at latitude ϕ is given as $P = \frac{\pi}{\Omega \sin \phi}$ where Ω is the rate of the earth's rotation. At latitude 40.5°N, the approximate location of the stations, the period for an inertial oscillation is 18.48 hours, coinciding closely with the observed peaks at both stations having a period of 18.7 hours.

Chiu (1973), using eight years of daily average wind data, found that at Denver, Colorado, the north-south wind spectrum peaks at or near 0.21 cycles per day (cpd) at upper levels of 700, 500, 300, 200, 100 and 50 mb. In addition, consistent peaks in the frequency interval from 0.20-0.25 cpd were observed at all upper levels at various other stations in the United States: Anchorage, Alaska; International Falls, Minnesota; Caribou, Maine; and Washington, D.C. Chiu suggested that these peaks are related to cyclones since cyclones have periods of five to seven days.

This particular peak at 0.21 cpd at Denver has a period of five days. The maximum peak observed at station 622 has a period of six days while that at station 421 has a period of nine days. Again, these peaks may be due to insufficient data points. Nevertheless, they could be the same peak observed by Chiu.

F. Cospectrum Analysis

In order to determine how the two time series are related to each other, a cross spectral analysis is performed by calculating the cross covariances:

$$r'_L = \frac{\overline{X_t Y_{t+L}} - \bar{X}\,\bar{Y}}{S_x S_y}$$

where X is given by the series at station 622 and Y is given by the series at station 421 (Tables 16 and 17); L is the lag and S_x^2 and S_y^2 are total variances for X and Y respectively. The cospectrum is computed by first averaging the cross covariances at lag L and lag $-L$. The series of these mean cross covariances is subjected to the power spectral analysis method as outlined in the previous section (Equations 1-3).

Autocorrelation coefficients are plotted over time lag and the cospectrum is plotted over frequency (Figures 12 and 13). The longest lag is 96 hours. Thus, the fundamental period is eight days, the second harmonic has a period of four days, and so on. The only real peak has a period of eight days. The secondary peak has a period of $2m/11$ or 17.5 hours. An inertial period has been found to be 18.5 hours. This eight day peak could again be related to cyclones while the peak at 17.5 hours suggests the influence of inertial oscillations.

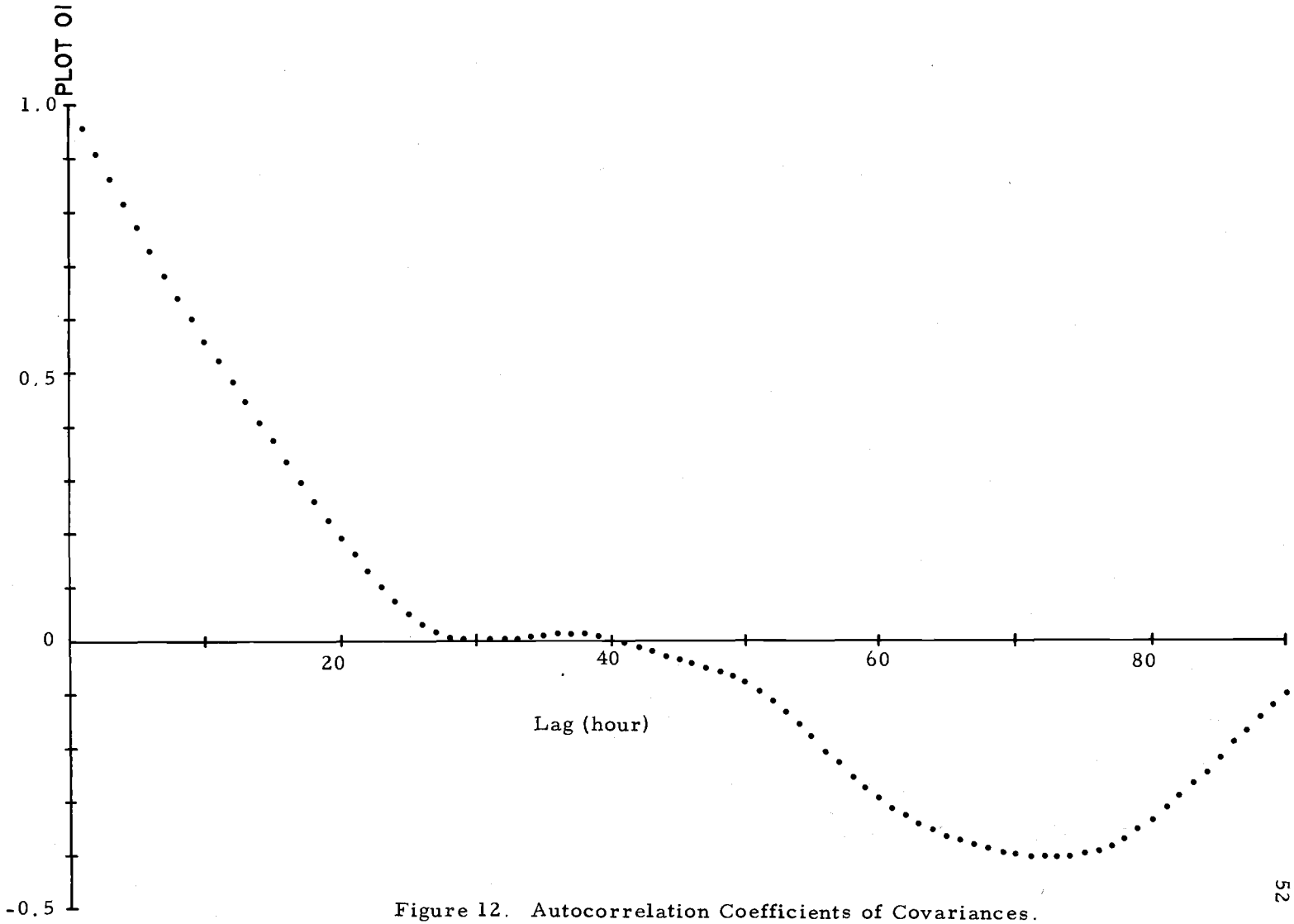

Figure 12. Autocorrelation Coefficients of Covariances.

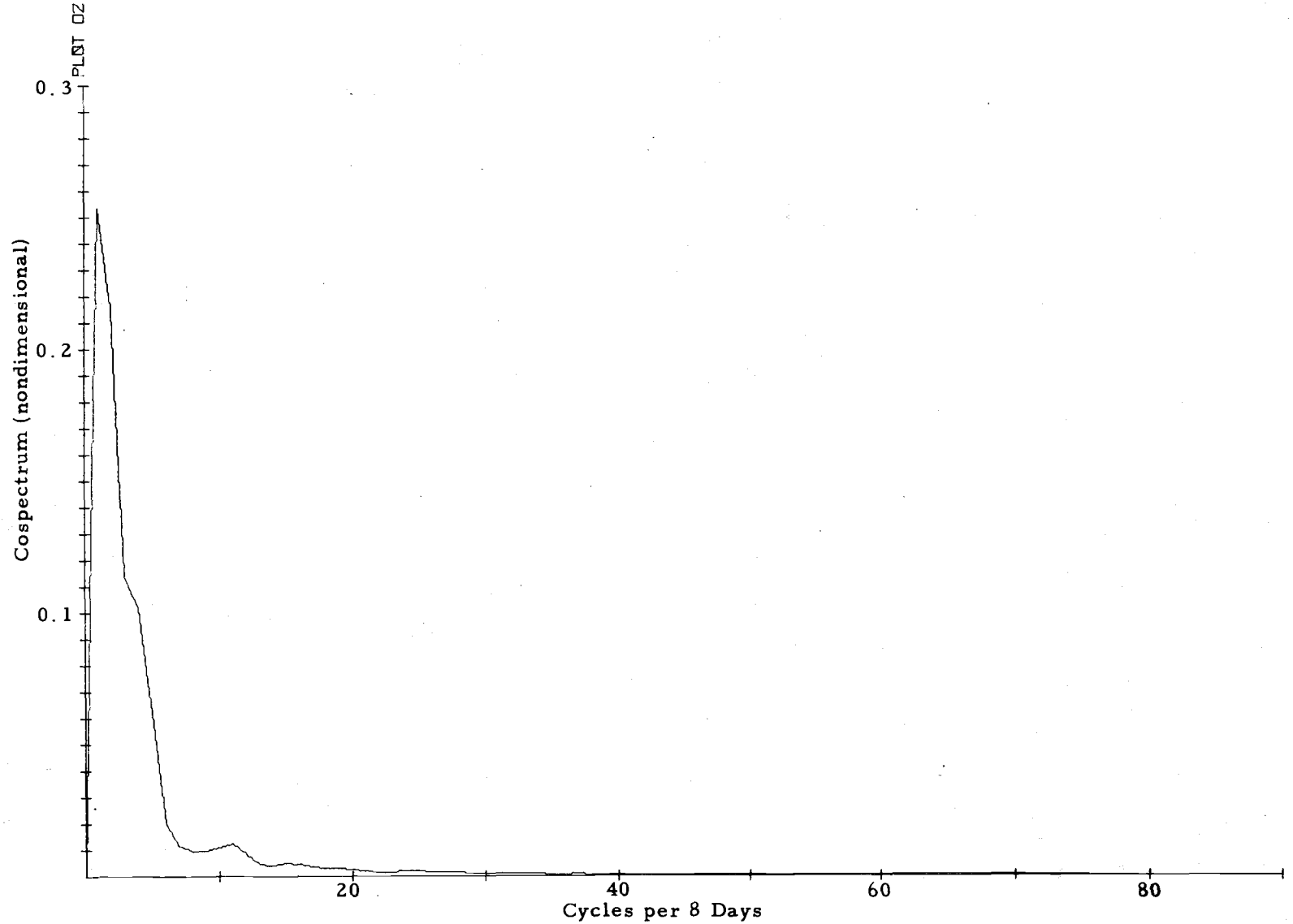

Figure 13. Cospectrum for Stations 421 and 622.

The high frequency end of the cospectrum curve is magnified to see if peaks having periods in the order of hours exist. From Figure 14, peaks do occur at frequencies of 37, 64, 73, 79 cycles/8 days. Periods corresponding to these frequencies are 5.2, 3, 2.6, and 2.4 hours. These may be connected with inertial gravity waves or thunderstorms.

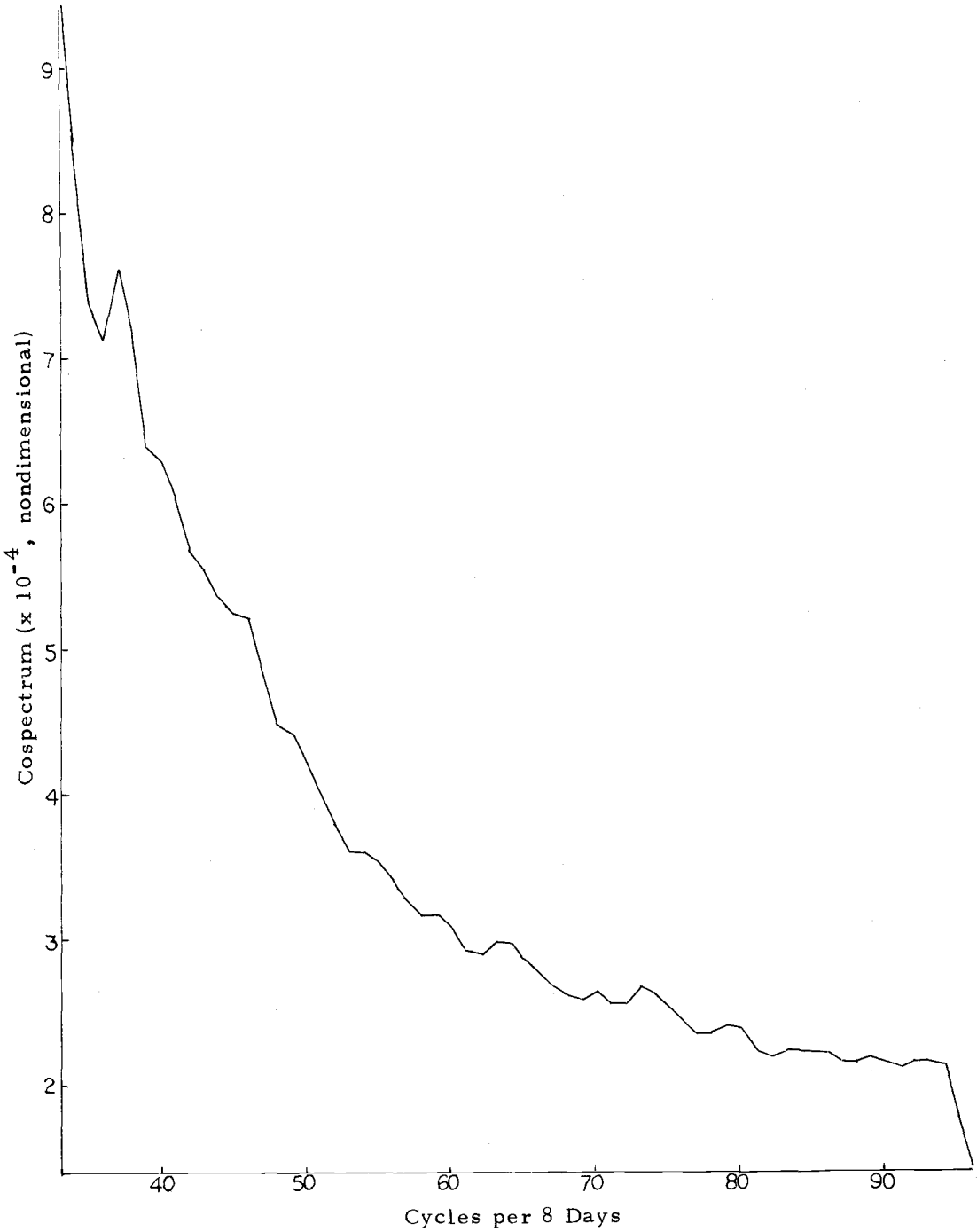

Figure 14. High Frequency End of Cospectrum.

V. SUMMARY AND CONCLUSIONS

Surface temperature, pressure, wind direction and speed readings collected at six stations in a mesonetwork in Colorado during July 1973 by the National Hail Research Experiment are analyzed. These six stations lie in a straight line in a north-south direction.

The stability analysis shows that the potential temperature at a station of higher elevation is almost always greater than the potential temperature at a lower station. This indicates that air above the slope is stable most of the time. Further statistical calculations confirm that air along the slope is always stably stratified at night and is stably stratified over 75% of the daytime. The air flow along the slope cannot be guaranteed to be hydrostatic because the temperature field is not at steady state. Thus, a parcel of air moving down the slope would see a different temperature field than the instantaneous temperature field at the beginning of its ascent because the time scale for the adjustment of temperature is of the same order of magnitude as the time it takes for the parcel to travel down a slope. The air flow is not hydrostatic everywhere because vertical motions and therefore local vertical accelerations are implied by upslope-downslope flow. Nonetheless, nighttime downslope flow appears to be at least partly driven by hydrostatic baroclinic horizontal pressure gradients associated with diabatic heating on sloping terrain.

This is in agreement with Holton's theoretical prediction (1967) that the baroclinic part of the horizontal pressure gradient force is responsible for the boundary layer wind oscillation over the sloped Great Plains. However, it has to be pointed out that Houlton's prediction is based on low Rossby number flow. This means that the baroclinic part of the flow is more parallel than perpendicular to the slope. The observed flow at the NHRE mesonetwork has a high Rossby number which means that the flow is possibly more perpendicular than parallel to the slope partly due to large accelerations.

Differences in horizontal potential temperature, assuming a well mixed planetary boundary layer, are noticeable during late morning and early afternoon. In other words, baroclinic circulation due to local heating over sloping terrain is important only during that time period. Thermally generated local circulations transport heat, thus reducing the gradient in horizontal potential temperature. By mid and late afternoon, when hail activity is at a statistical maximum, differences in horizontal potential temperature are at a minimum.

Analysis of wind data shows that air moves upslope during the afternoon and downslope at night. Sub-diurnal oscillations present themselves in the hodographs constructed from observed wind velocities. These oscillations may be due to the coupling between the temperature field and the wind field. The maximum daytime speed occurs at 1700 and the maximum nighttime speed at 0500. In contrast,

Estoque's numerical work indicates that maximum wind speeds over flat terrain occur at 1300 local time. NHRE winds contrast also with Krishna's theoretical work that low level wind over flat terrain reaches a maximum before midnight and drops to a minimum by sunrise. The observed air movement over the NHRE mesonetwork is partly attributed to baroclinity caused by diurnal heating along a sloping terrain. The stability analysis seems to disprove the belief that upslope wind is generated by local instability resulting from non-hydrostatic buoyancy. This upslope flow is also influenced by synoptic scale effects and a downward mixing of momentum from aloft. Synoptic scale used here indicates a large spatial scale rather than a large temporal scale.

Spectral analysis of wind speeds shows numerous peaks and valleys in the spectra. Peaks are found to appear at frequencies of about 3, 10, 19, 23, 32, 40 and 53 cycles/9 days. Those having a period of 23 hours are attributed to diurnal oscillations and those having a period of 18 hours to inertial oscillations. The existence of other peaks is probably not statistically significant due to the limited number of data points. However, speculations as to their physical origin can still be made. Some of them are:

1) Superposition of thermal winds due to 50 km scale and 1000 km scale slope.
2) Gravity inertial waves.
3) Quasi-stationary waves shed from the Rockies.

BIBLIOGRAPHY

Atmospheric Technology, 4, December 1973: National Center for Atmospheric Research, Boulder, Colorado, 40 pp.

Blackman, R. B. and J. W. Tukey, 1958: The Measurement of Power Spectra. New York, Dover, 190 pp.

Bonner, W. D. and J. Paegle, 1970: Diurnal variations in boundary layer winds over the South Central United States in summer. Monthly Weather Review, 98, 735-744.

Brooks, P. and N. Carruthers, 1953: Handbook of Statistical Methods in Meteorology. London, Her Majesty's Stationery Office, 412 pp.

Chapman and Lindzen, 1970: Atmospheric Tides. New York, Science Publishers.

Churchill, R. V., 1969: Fourier Series and Boundary Value Problems. New York, McGraw-Hill Book Company, 248 pp.

Chiu, Wan-Cheng, 1973: On the atmospheric kinetic energy spectrum and its estimation at some selected stations. Journal of Atmospheric Sciences, 30, 377-391.

Crawford, K. C. and H. R. Hudson, 1972: The diurnal wind variation in the lowest 1500 feet in Central Oklahoma: June 1966-May 1967. Journal of Applied Meteorology, 12, 127-132.

Dixon, W. J. and F. J. Massey, 1957: Introduction to Statistical Analysis. New York, McGraw-Hill Book Company.

Estoque, M., 1963: A numerical model of atmospheric boundary layer. Journal of Geophysical Research, 68, 1103-1113.

Frenzel, C. W., 1962: Diurnal wind variations in Central California. Journal of Applied Meteorology, 1, 405-414.

Geiger, R., 1957: The Climate Near the Ground. Massachusetts, Harvard University Press, 494 pp.

Hess, S. L., 1959: Introduction to Theoretical Meteorology. New York, Holt, Rinehart and Winston, 362 pp.

Hisdal, V., 1972: Diurnal wind variation in Antartica. Quarterly Journal of Royal Meteorological Society, 98, 673-680.

Holton, J.R., 1967: The diurnal boundary layer wind oscillation above sloping terrain. Tellus, 19, 199-205.

_____, 1972: An Introduction to Dynamic Meteorology. New York, Academic Press, 319 pp.

Krishna, K., 1968: A numerical study of diurnal variation of meteorological parameters in the planetary boundary layer. Monthly Weather Review, 96, 267-276.

MacHattie, L.B., 1967: Kananaskis Valley winds in summer. Journal of Applied Meteorology, 6, 348-352.

National Hail Research Experiment Program Plan 1972-1976, 1972: National Center for Atmospheric Research, Boulder, Colorado, 135 pp.

Paegle, J., 1970: Studies of diurnally periodic boundary layer winds. Technical Report to the National Science Foundation, Department of Meteorology, UCLA.

Panofsky, H.A. and G.W. Brier, 1965: Some Applications of Statistics to Meteorology, 126-161 pp.

Simpson, G.C., 1918: The 12-hourly barometer oscillation. Quarterly Journal of Royal Meteorological Society, 44, 1-19.

The National Hail Research Experiment Summer 1972 Summary Report. Technical Report No. 72/2, 1972: National Center for Atmospheric Research, Boulder, Colorado, 92 pp.

Yu, T. and N.K. Wagner, 1970: Diurnal variation of onshore wind speed near a coastline. Journal of Applied Meteorology, 9, 760-766.